JOINT TRANSPORTATION
RESEARCH PROGRAM
INDIANA DEPARTMENT OF TRANSPORTATION
AND PURDUE UNIVERSITY

Physics-Based Modelling of Concrete Degradation Phenomena: Impact of Construction Defects on Long Term Cost and Material Properties

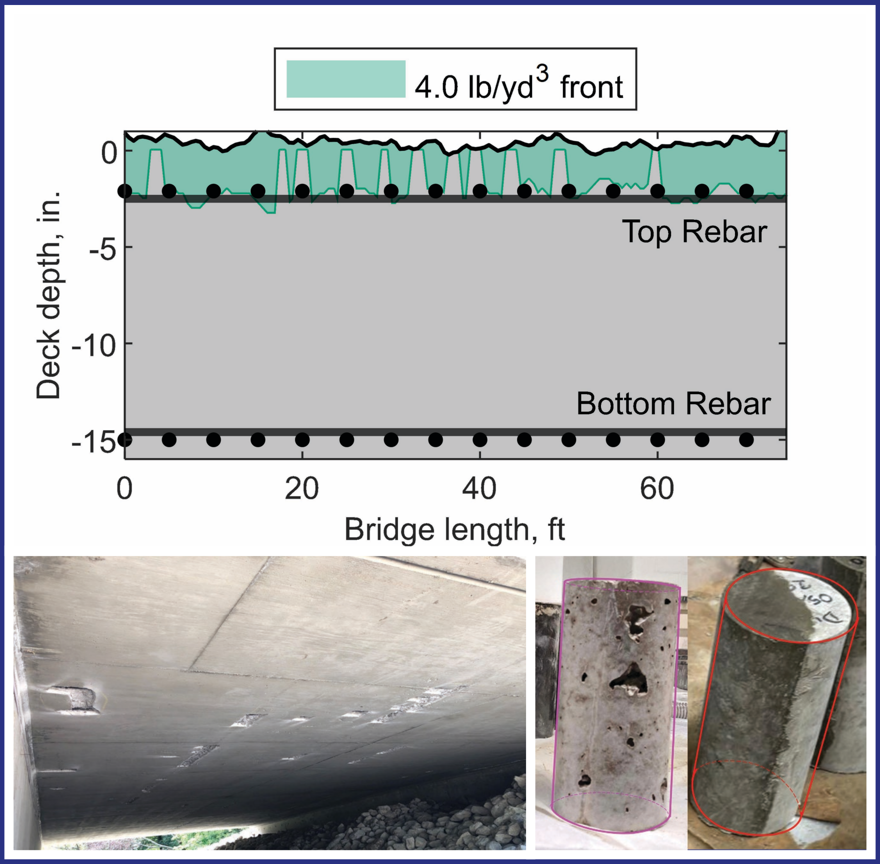

Manuel Salmeron, Oscar Forero, Talha Faiz,
Kabir Shrivastava, Shirley J. Dyke, and Julio A. Ramirez

SPR-4840 • Report Number: FHWA/IN/JTRP-2026/14 • DOI: 10.5703/1288284318622

RECOMMENDED CITATION

Salmeron, M., Forero, O., Faiz, T., Shrivastava, K., Dyke, S. J., & Ramirez, J. A. (2026). *Physics-based modelling of concrete degradation phenomena: Impact of construction defects on long term cost and material properties* (Joint Transportation Research Program Publication No. FHWA/IN/JTRP-2026/14). West Lafayette, IN: Purdue University. https://doi.org/10.5703/1288284318622

AUTHORS

Manuel Salmeron
Purdue University
(765) 476-3284
salmeron@purdue.edu
Corresponding Author

Oscar Forero
Graduate Research Assistant
Lyles School of Civil and Construction Engineering
Purdue University

Talha Faiz
Graduate Research Assistant
Lyles School of Civil and Construction Engineering
Purdue University

Kabir Shrivastava
Undergraduate Research Assistant
School of Mechanical Engineering
Purdue University

Shirley J. Dyke, PhD
Donald and Patricia Coates Professor of Innovation
School of Mechanical Engineering
Purdue University
(765) 494-7434
sdyke@purdue.edu

Julio A. Ramirez, PhD
Kettelhut Professor of Civil Engineer and
NHERI-NCO Center Director
Lyles School of Civil and Construction Engineering
Purdue University
(765) 494-2716
ramirez@purdue.edu

JOINT TRANSPORTATION RESEARCH PROGRAM

The Joint Transportation Research Program serves as a vehicle for INDOT collaboration with higher education institutions and industry in Indiana to facilitate innovation that results in continuous improvement in the planning, design, construction, operation, management and economic efficiency of the Indiana transportation infrastructure. Learn more at engineering.purdue.edu/JTRP.

Published reports of the Joint Transportation Research Program are available at docs.lib.purdue.edu/jtrp/.

NOTICE

TECHNICAL REPORT DOCUMENTATION PAGE

<table>
<tr><td>1. Report No.
FHWA/IN/JTRP-2026/14</td><td>2. Government Accession No.</td><td>3. Recipient's Catalog No.</td></tr>
<tr><td colspan="2">4. Title and Subtitle
Physics-based modelling of concrete degradation phenomena: Impact of construction defects on long term cost and material properties</td><td>5. Report Date
February 27, 2026
6. Performing Organization Code</td></tr>
<tr><td colspan="2">7. Author(s)
Manuel Salmeron (https://orcid.org/0000-0001-7262-7652)
Oscar Forero (https://orcid.org/0009-0000-9186-8064)
Talha Faiz (https://orcid.org/0009-0003-4468-6614)
Kabir Shrivastava (https://orcid.org/0009-0004-2845-3842)
Shirley J. Dyke, PhD (https://orcid.org/0000-0003-3697-992X)
Julio A. Ramirez, PhD (https://orcid.org/0000-0002-7057-4240)</td><td>8. Performing Organization Report No.
FHWA/IN/JTRP-2026/14</td></tr>
<tr><td colspan="2">9. Performing Organization Name and Address
Joint Transportation Research Program
Hall for Discovery and Learning Research (DLR), Suite 204
207 S. Martin Jischke Drive
West Lafayette, IN 47907</td><td>10. Work Unit No.
11. Contract or Grant No.
SPR-4840</td></tr>
<tr><td colspan="2">12. Sponsoring Agency Name and Address
Indiana Department of Transportation (SPR)
State Office Building
100 North Senate Avenue
Indianapolis, IN 46204</td><td>13. Type of Report and Period Covered
Final Report
14. Sponsoring Agency Code</td></tr>
<tr><td colspan="3">15. Supplementary Notes
Conducted in cooperation with the U.S. Department of Transportation, Federal Highway Administration.</td></tr>
<tr><td colspan="3">16. Abstract
The quality of workmanship and adherence to specifications during the bridge construction phase of concrete decks, slabs, and continuous T-beams, are key factors on which future structural performance and durability hinge. If construction practices do not meet the required standards of quality, they may trigger early onset of deterioration processes that shorten the service life leading to unplanned interventions or unscheduled repairs, thus intensifying the need for maintenance actions and increasing costs during the service life of the bridge. Despite the consensus view that substandard construction practices reduce the performance of concrete structures, quantifying the impact is challenging. This difficulty is owed to the various deterioration processes involved that can be quite complex and have significant uncertainty, and to the challenge in accurately establishing the initial condition of the bridge.
In this project, the research team from Purdue University expands the framework developed in SPR-4526 by incorporating the quantification of service life and costs associated with the loss in durability and structural performance in the presence of an excessive amount of air voids. The effect of interventions and repairs on recovering the loss of life, and their added costs, are also quantified.</td></tr>
<tr><td colspan="2">17. Key Words
corrosion, life expectancy, bridge decks, chlorides, durability, construction and maintenance, air voids, deterioration, life cycle costing, physics-based mode</td><td>18. Distribution Statement
No restrictions. This document is available through the National Technical Information Service, Springfield, VA 22161.</td></tr>
</table>

19. Security Classif. (of this report)	20. Security Classif. (of this page)	21. No. of Pages	22. Price
Unclassified	Unclassified	35	

Form DOT F 1700.7 (8-72) Reproduction of completed page authorized

EXECUTIVE SUMMARY

Introduction

The Indiana State Department of Transportation (INDOT), like other state departments of transportation, recognizes that workmanship quality and adherence to specifications during concrete deck construction are critical to long-term durability and structural performance. Substandard construction practices can result in early deterioration and shortened service life and can lead to unplanned repairs, thereby increasing maintenance needs and lifecycle costs. Predicting the service life of bridges with 8-in.-thick girder-supported reinforced concrete decks, one-way solid continuous slab, or T-beam bridge systems, remains challenging due to the complexity and uncertainty of deterioration processes and the difficulty in accurately defining initial bridge conditions. In this project, the research team from Purdue University expands the framework developed in SPR-4526 (Criner et al., 2023) by incorporating the quantification of service life and costs associated with the loss in durability and structural performance in the presence of air voids. The effect of interventions and repairs on recovering the loss of life, and their added costs, are also quantified.

Findings

- This study provides a quantitative approach to estimate the service life of bridge decks, one-way continuous solid slab and T-beam bridge systems, thus enabling INDOT to evaluate several key metrics such as chloride penetration, degree of bar corrosion, and the influence of the presence of voids and interventions, and to also assess economic losses associated with the premature deterioration of concrete decks.
- A model-based process is developed to support decision makers in making informed choices regarding investments and maintenance strategies.
- Results indicate that improved planning informed by the physics-based model developed can reduce the need for unplanned repairs and interventions, thus improving traffic flow and overall mobility for roadway users.
- Numerical modeling based on the best available understanding of the relevant physics corroborates the expectation that defective construction practices may significantly accelerate deterioration processes, shorten the service life of concrete bridges within the scope of this study, and increase the likelihood of unplanned interventions.
- A more accurate prediction of future bridge condition would require understanding long-term trends in time-dependent deterioration parameters, such as chloride profiles, corrosion current densities, and crack widths, which cannot be reliably captured through laboratory testing alone and are best obtained through long-term monitoring.

Implementation

The findings of this research are intended to be implemented through a model-based decision-support framework that assists INDOT in evaluating bridge deck deterioration and maintenance strategies. The refined model extends prior work by enabling long-term simulation of bridge performance over the entire service life. Rather than considering just a single point in the deck, the model captures the deterioration of a strip along the length of the deck. The framework can predict condition ratings, visible cracking, loss of structural capacity, maintenance needs, and associated costs while accounting for inherent variabilities. This capability facilitates condition- and cost-based comparisons of alternative scenarios as well as an assessment of how typical uncertainties influence outcomes.

A key implementation step is the use of the model to evaluate and compare maintenance schedules and intervention strategies. Users can define intervention schedules based on either agency experience or target performance thresholds, and the model automatically simulates how these actions influence deterioration over time. This capability supports informed selection of maintenance strategies that balance performance objectives and resource constraints. The model also supports direct comparisons between well-constructed bridges and those affected by early-age void defects, highlighting the long-term consequences of construction quality on deterioration rates, structural capacity loss, and lifecycle costs.

The framework is intended to support planning and asset-management rather than as a substitute for detailed inspections or formal economic analyses. Its primary role is to enable relative comparisons among scenarios, guide prioritization of maintenance actions, and improve long-term investment decisions.

For full implementation, a dedicated follow-up project is recommended to transition the current MATLAB-based methodology into a user-friendly application suitable for decision makers. This effort would include compiling scripts into an accessible interface, optimizing code execution, automating scenario selection, and developing a user manual that clearly defines required inputs and data collection procedures. Once implemented, the tool would allow INDOT personnel to routinely analyze bridge decks, evaluate intervention schedules, and assess the impacts of construction defects, thereby integrating the research findings into everyday asset management practice. Samples of actual applications could be selected in consultation with INDOT personnel to illustrate the implemented framework.

CONTENTS

LIST OF TABLES

LIST OF FIGURES

1. INTRODUCTION

The service life of bridges with an 8-in. reinforced concrete deck over girders, one-way continuous solid slab, or a continuous T-beam, taken as the number of years that it will be used for its intended purpose within appropriate performance requirements (ACI Committee 365, 2017), depends on several key factors. It is understood by the Indiana Department of Transportation (INDOT) as well as other state departments of transportation that the quality of workmanship and adherence to specifications during the construction phase of a concrete deck are key factors on which the future structural performance and durability hinge.

If construction practices do not meet the required standards of quality, they may trigger early onset of deterioration processes that shorten the service life leading to unplanned interventions or unscheduled repairs, thus accelerating the need for maintenance actions and increasing costs during the service life of the bridge. Despite the consensus view that substandard construction practices reduce the performance of concrete deck and one-way slab and T-beam bridges, quantifying the impact is challenging. This difficulty is owed to the various deterioration processes involved that can be quite complex and have significant uncertainty and to the inherent difficulty in accurately establishing the initial condition of the bridge.

In this project, the research team from Purdue University expands the framework developed in SPR-4526 (Criner et al., 2023) by incorporating the quantification of service life and costs associated with the loss in durability and structural performance in the presence of air voids. The effect of interventions and repairs on recovering the loss of life, and their added costs, are also quantified.

1.1 Scope

Here, the focus is on evaluating the impact on the service life and associated costs of excessive number of air voids and large-sized voids, colloquially known as "honeycombs," and effectiveness of intervention strategies and repairs in extending the service life of structures without voids and recovering the service life of structures with voids. Three interventions are considered: thin deck overlays, rigid deck overlays, and patching.

The individual models developed in this study are validated using available data and integrated into a comprehensive methodology. The methodology is then used to compare the performance of nonstandard structures and standard structures that have undergone corrective interventions. This comparison provides insight into how construction quality and intervention strategies influence bridge deck performance, durability, and lifecycle costs.

The long-term deterioration processes modeled in this project include corrosion and progressive cracking in the surface of the deck caused by fatigue, shrinkage, or other phenomena affecting the concrete surface. Delamination and spalling are outside the scope.

The structural components considered in this project as agreed upon with the Study Advisory Committee include: 8-in.-thick concrete bridge decks supported on steel, or prestressed concrete girders, one-way solid concrete slabs continuous and simply supported, and continuous reinforced concrete T-beam bridges.

1.2 Corrosion-Induced Deterioration

The effect of corrosion of reinforcement is evaluated in terms of cracking and stiffness degradation during its service life, as well as on the ultimate flexural, shear and bond strength. Reinforcement corrosion is deemed the main threat to durability in reinforced concrete bridges (Poursaee, 2016). This assessment is because corrosion-induced cracks are major drivers of further chloride and moisture ingress, exacerbating existing corrosion and leading to spalling. The overall reduction in stiffness may cause deflections that exceed the serviceability limits. Corrosion reduces the rebar cross-section as well as the steel and concrete strength, which in turn may decrease the load carrying capacity of the structure. Ultimately these changes may undermine the bond between the concrete and steel.

Steel reinforcement embedded in concrete is protected against corrosion by a hydroxide barrier layer of ferrous compounds (Poursaee, 2016). A high accumulation of chlorides, contained mainly in water mixed with deicing salts, breaks the protective layer in a process known as depassivation. Once depassivation has occurred, the corrosion process starts. Although greatly reduced by epoxy coating, corrosion may develop in bar locations where the coating has been damaged or delaminated due to improper fabrication, handling, or storage during construction (Samples & Ramirez, 2000). When present, due to the increased volume from corrosion by-products these may increase tensile strains in the concrete surrounding the rebar. Eventually, the strains surpass the tensile strength of the concrete, leading to cracking of the concrete cover. Cracks then become points of ingress for water and other substances, which increase the likelihood of the corrosion process spreading to neighboring regions of the bridge deck.

2. INTERVENTIONS

Interventions are critical to the lifecycle of a bridge. If the construction of the bridge has been performed following standard procedures, then the interventions can be preventive in nature and are meant to ensure that the bridge reaches its design service life. Instead, if nonstandard construction has been used, then the interventions are labeled as corrective. The effectiveness of an intervention to improve the performance level of a structure depends on the quality of its implementation, as well as on the state of deterioration and the time of application in the lifecycle of the intervened bridge. Three interventions are evaluated in this project: (1) thin deck overlays, (2) rigid deck overlays, and (3) patches.

2.1 Definitions and Procedures

INDOT's definitions of the interventions that are within the scope of this project are presented and common placement criteria and practices are described in this section.

2.1.1 Thin Deck Overlays

Thin deck overlays, also known as flexible overlays, polymeric overlays, or epoxy overlays, are preventive maintenance strategies that extend the service life of bridge decks and slabs by addressing minor deterioration and preventing chloride intrusion. Typically, thin deck overlays are 3/8 in. (9.5 mm) thick and are applied over the existing surface of a bridge deck. According to INDOT's (2020) *Bridge Design Aids* (BDA) 412-03, overlays are most effective when applied to decks that have minimal cracking and delamination, with less than 5% of the surface area affected by spalls or delamination, and having anticipated patching limited to no more than 10% of the area. Alternatively, the *Indiana Design Manual* (INDOT, 2013) indicates a maximum anticipated patching area of 15%.

The application of a thin deck overlay is viewed as a preventive practice. According to INDOT's experience, the average time for the placement of the first thin deck overlay is around 10 years after the construction of the original deck. A thin deck overlay is applied to a bridge deck that shows cracking, but where the damage is not enough to justify a more intensive type of intervention. A second thin deck overlay is then placed around 10 years after the first one, that is, 20 years after the construction of the deck. However, in the presence of early cracking, that is, cracks appearing 2 to 5 years after construction, the application of the first thin deck overlay can be sooner, at 7 years. In an ideally performing deck, the first thin deck overlay would be placed 15 years from construction, but typically, the first application occurs at 10 years from construction. The second thin overlay application occurs 15 years after the first one in most decks. Preventive measures are prioritized over rehabilitation; therefore, this technique is not recommended for decks with either extensive chloride presence or cracking and/or spalling.

The application procedure for a thin deck overlay consists of:

1. Perform shot blasting over the deck to create a roughened surface.
2. Flood the roughened surface with the selected epoxy material, which is spread using squeegees. Apply crushed limestone as the epoxy material is spread over the deck.
3. Remove the excess stone with an air hose and a broom truck.
4. Repeat the procedure a second time.

2.1.2 Rigid Deck Overlays

Contrary to thin deck overlays, rigid deck overlays address major deterioration due to cracking, delamination, spalling, or debonding. The criterion for applying a rigid overlay is condition-based, with condition rating (CR) 6 being the typical threshold for application. According to the *Indiana Design Manual* (INDOT, 2013), the minimum thickness of a rigid deck overlay should be 1.5 in. (38.1 mm), with 1.75 in. (44.45 mm) being the desirable thickness. Rigid overlays thicker than 3 in. (76.2 mm) require approval. In general, thicker overlays are more likely to have shrinkage cracking.

The *Indiana Design Manual* (INDOT, 2013) mentions a minimum life expectancy of 15 years for rigid deck overlays, which agrees with the typical 20-year mark indicated by INDOT personnel interviewed for this project. A second rigid deck overlay is indicated after the previously existing and already deteriorated overlay has been removed. The second rigid overlay is expected to have a shorter lifetime; 15 to 20 years is the usual target. The lifetime of a rigid overlay is strongly influenced by the average daily traffic (ADT). For example, for overlays placed on interstate bridges, which have high ADTs, durations of 15 to 17 years are typical. A third rigid deck overlay is not recommended due to the likelihood of needing extensive patching. Any bridge deck requiring patching of more than 35% of the deck area should be replaced.

The procedure for placing a rigid deck overlay includes milling of the existing deck, which is usually either a thin overlay or a previous rigid overlay. A rigid deck overlay is rarely placed on the original deck. The milling depth is usually 1/4 in. to 1/2 in. (6.35 mm to 12.7 mm). After milling, weak concrete is removed by hydro-demolition and hand-chipping, and patching is applied wherever necessary. Finally, the new rigid deck overlay is placed.

2.1.3 Patches

Patching is widely used in bridge deck repairs. Patching can be used for nonstructural or cosmetic repairs, improving resistance to abrasion, improving the appearance of the surface, protecting rebars against corrosion and fire, or reducing permeability. In such repairs, typically the patch should have adequate strength to work together with the existing concrete without delaminating. Hence, design of such patches is intended to ensure that the bond strength at the interface is greater than the stress at the interface. In structural repairs, the patch is required to carry the load originally carried by the removed concrete and to allow for any volumetric changes that may occur over time. Structural patch repairs can restore the design strength of a damaged member or improve the capacity of a substandard member.

The findings from Al-Salloum (2007), Beushausen and Alexander (2007), Cusson (2009), Czarnecki et al. (2020), Do and Kim (2012), Emberson and Mays (1996), Kiani et al. (2018), Kristiawan et al. (2016, 2021), Malumbela et al. (2011), Manawadu et al. (2023), Mangat and O'Flaherty (2000), Morgan (1996), Nounu and Chaudhary (1999), Pattnaik and Rangaraju (2007), Pellegrino et al. (2011), Sahamitmongkol et al. (2008), and Teixeira et al. (2019) were used to establish the impact of patch repairs on the flexural strength of reinforced concrete beams. Using compatible patching materials, whether applied in the tension or compression regions of a member, has been shown to restore or enhance the structural strength of noncorroded reinforced concrete beams, in flexure, shear, and bond. Although patching a corroded reinforced concrete beam improves its structural capacity as compared to that of an unrepaired corroded beam, the strength of the repaired beam typically does not exceed the strength of noncorroded control beams in the studies. This behavior can be attributed to the fact that the cross-section of steel reinforcement that is lost due to corrosion is not recovered. Key factors such as the compatibility of the repair material with the substrate, as well as the bond strength, patch thickness, and length will significantly influence the overall beam strength. In general, patch repairs may not only improve a beam's strength, but they also help reduce the amount of cracking. Bridge decks can be viewed as beams for structural strength purposes by assuming an effective width; therefore, this reasoning can also be used to understand the effects of repairs on reinforced concrete bridge decks.

2.2 Structural Performance

The impact of deterioration from corrosion on the structural performance of reinforced concrete flexural members can be classified into effects on the steel, the concrete, and the bond between the steel and concrete. Corrosion of the reinforcement causes a loss of mass in steel bars, which reduces the effective area of the steel cross-section. The yield strength of the reinforcement is also reduced in a linear fashion as a function of rebar corrosion (Stewart & Al-Harthy, 2008). Corrosion of the bars also deteriorates the bond strength between the bar and concrete as a function of the extent of bar corrosion, the size of the bar, and the concrete cover. The reduction in bond strength competes with the reduction in yield strength and area loss and may be a governing factor in the flexural strength when the bond strength becomes insufficient to develop the bar yield strength. Reinforcement corrosion affects the concrete around it by inducing cracks due to the formation of corrosion products, eventually leading to spalling of the concrete cover. The corrosion cracks induced in concrete due to the expansion of rust products can reduce the concrete strength.

2.2.1 Flexural Strength Deterioration

In this study, a critical section for flexural strength deterioration is defined as the section that tends to deteriorate faster with respect to corrosion and where the flexural demand is high in the tension reinforcement. As the chloride salts diffuse through the top surface, the reinforcement closer to the surface is more susceptible to corrosion damage. Keeping this in mind, the negative moment regions in the bridge deck, and continuous one-way solid slab and T-beam bridges which have the structural tension reinforcement at the top, tend to be critical as they are more prone to corrosion damage. Figure 2.1 shows the free body diagram for a section in the negative moment region with tension at the top of the section and compression at the bottom, where b is the cross-section width, c is the depth of the neutral axis, T_s is the tension force available in the rebars, f_y is the yield strength of the rebar, A_{st} is the area of the rebars, f_c is the compressive stress distribution following the Hognestad parabola, and C_{con} is the compressive force.

In the section shown in Figure 2.1, reinforcing bar corrosion is assumed that affects its yield strength linearly as a function of steel sectional loss, given as:

$$f_y^* = \left(1 - \alpha_y m_l\right) f_y \qquad \text{Equation 2.1}$$

where f_y^* s the yield strength of the corroded rebar, f_y is the original yield strength of the rebar, m_l is the corrosion mass loss in percentage (corrosion level) of the corroded rebar to

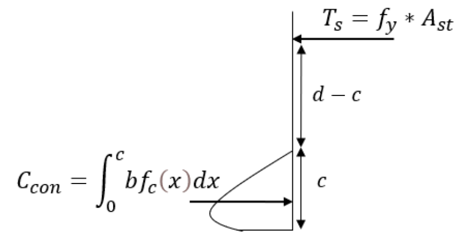

Figure 2.1 Internal Forces in the Critical Cross-Section.

the original rebar, and α_y is an empirical coefficient. Different empirical coefficients have been proposed by several authors (Cairns et al., 2005; Du et al., 2005; Imperatore et al., 2017). However, herein the value of α_y is taken as 0.005, as proposed by Du et al. (2005).

The corroded area, A_{st}^*, of the reinforcement is calculated by modifying the original noncorroded area, A_{st}, as follows:

$$A_{st}^* = A_{st} - \frac{\pi}{4} D_r^{\,2}\left(m_l\right) \qquad \text{Equation 2.2}$$

where $D_r\left(m_l\right)$ is the diameter of corroded rebar as a function of corrosion level. The reduced tensile force in the rebar due to corrosion is estimated as the product of Equation 2.1 and Equation 2.2. The reduction is bond strength due to corrosion is estimated using the equation proposed by Han et al. (2022) as follows:

$$\tau_{max} = \begin{cases} \tau_0 & m_l < m_{l_1} \\ \tau_0[1 - k_1 \operatorname{erf}\left(k_2 m_l\right)] & m_l \geq m_{l_1} \end{cases} \qquad \text{Equation 2.3}$$

where m_{l_1}, represents the threshold corrosion level, k_1 and k_2 are empirical constants. All three parameters depend on the cover-to-diameter ratio C_x / d_b, as shown in Figure 7 of Han et al. (2022). Additionally, τ_{max} is the bond stress in the corroded rebar, and τ_0 is the original bond stress in the rebar, determined by:

$$\tau_0 = 0.35 f_c' \left(\frac{C_x}{d_b}\right)^{0.21} \qquad \text{Equation 2.4}$$

The yield strength in the tension rebars is developed provided they have sufficient bond strength. As the corrosion in the tension rebars increases, the bond strength may not be sufficient for the rebars to develop yield strength (Han et al., 2022). The flexure strength and the failure mechanism in this case are thus governed by bond strength. The maximum tension force in the corroded reinforcement is therefore estimated as follows:

$$T_{s,corr} = min\left(f_y^* A_{st}^*, \tau_{max}\, n\pi\, d_b^* l_d\right) \qquad \text{Equation 2.5}$$

where $T_{s,corr}$ is the tension force available in the corroded rebars, d_b^* is the diameter of the corroded tension rebar, and l_d is the development length of the rebars, determined from construction drawings, field investigation, or code-based estimates.

The flexural strength of the corroded reinforced concrete section is determined by calculating the depth of the neutral axis, c, first, for which an iterative approach to solve the force equilibrium is adopted, as follows:

$$T_{s,corr} = \int_0^c b\, f_c(x)\, dx \qquad \text{Equation 2.6}$$

where x is the distance starting from the neutral axis to the extreme top fiber of the section in compression, which is at an ultimate compressive strain (ε_{cm}) of 0.003, b is the width of the cross-section, $f_c(x)$ the compressive stress of the concrete at a distance x from the neutral axis. In this study, the Hognestad parabola is adopted as the stress model for $f_c(x)$. In the case in which bond strength is insufficient to develop yield strength, the tensile strain, ε_s, in the rebar is calculated as follows:

$$\varepsilon_s = \frac{\tau_{max}\ n\pi\ d_b\ l_d}{A_{sl}^{*} E_s} \qquad \text{Equation 2.7}$$

where E_s is the elastic modulus of the steel reinforcement. Defining d as the effective depth of the cross-section, the top fiber strain ε_{cm} in this case, is given by:

$$\varepsilon_{cm} = \varepsilon_s \frac{c}{d-c} \qquad \text{Equation 2.8}$$

The value of ε_{cm} should not exceed 0.003. After finding the neutral axis depth, c, by solving Equation 2.6, the centroid of the Hognestad parabola, where the total compressive force of the concrete acts, is calculated as:

$$x_c \int_0^c b f_c(x)\, dx = \int_0^c b f_c(x)\, x\, dx \qquad \text{Equation 2.9}$$

where x_c is the centroid of the parabola. The residual flexural strength, $M_{n,res}$, can be calculated as follows:

$$M_{n,res} = T_{s,corr} * (d - c + x_c) \qquad \text{Equation 2.10}$$

2.2.2 Shear Strength Deterioration

In this work, a sectional approach for reinforced concrete beams is used. With the sectional approach in beams, we adopt the American Concrete Institute (ACI) 318-19 equations for shear strength in 22.5.5 for V_c for non-prestressed members, and the equations in 22.5.8 for the contribution from stirrups V_s, to predict the residual shear strength of corroded reinforced concrete sections (ACI Committee 318, 2019).

The residual shear strength of the corroded reinforced concrete section is calculated based on the shear strength equation given in ACI 318-19. The nominal shear strength calculated using ACI 318-19 is as follows:

$$V_n = V_c + V_s \qquad \text{Equation 2.11}$$

where V_n is the nominal shear strength, V_c is the shear strength contribution from concrete, and V_s is the strength contribution from the shear reinforcements, or stirrups. V_s is calculated as:

$$V_s = \frac{A_v f_y d}{s}, \qquad \text{Equation 2.12}$$

where A_v is the area of stirrups, f_y is the yield strength of the stirrups, d is the effective depth of the cross-section, and s is the longitudinal spacing of stirrups.

2.2.2.1 Concrete Contribution in 8-in. Concrete Decks and Solid One-Way Slabs. The shear contribution from concrete, V_c, for non-prestressed members without stirrups is calculated using the expressions in Table 2.1.

TABLE 2.1
V_c for Non-Prestressed Members.

Criteria		V_c	
$A_v \geq A_{v,min}$		$\left[2\lambda\sqrt{f_c'} + \frac{N_u}{6A_g}\right] b_w d$	(a)
	Either of:	$\left[8\lambda(\rho_w)^{1/3}\sqrt{f_c'} + \frac{N_u}{6A_g}\right] b_w d$	(b)
$A_v < A_{v,min}$		$\left[8\lambda_s\lambda(\rho_w)^{1/3}\sqrt{f_c'} + \frac{N_u}{6A_g}\right] b_w d$	(c)

where ρ_w is the longitudinal reinforcement ratio, f_c' is the compressive strength of concrete, b_w is the web width, A_g is the gross sectional area, N_u is the axial load, λ is the correction factor related to unit weight of concrete, and λ_s is the modification factor for size effect given by:

$$\lambda_s = \sqrt{\frac{2}{1+\frac{d}{10}}} \leq 1 \qquad \text{Equation 2.13}$$

In Table 2.1, the value of $\frac{N_u}{6A_g}$ shall be less than $0.05 f_c'$ as per ACI 318-19 (ACI Committee 318, 2019). To calculate the residual shear strength of the corroded sections, the nominal shear strength equation given by ACI 318-19 is modified to incorporate the deterioration in the material properties affected by corrosion. In beams, N_u is taken equal to zero. For cross-sections taken from either a one-way continuous reinforced concrete slab deck or the 8 in.-thick deck over girder, as there are no structural stirrups present, the shear strength is only provided by concrete, V_c, and is calculated using the equation designated as c in Table 2.1. Due to corrosion, the reduction in the area of longitudinal reinforcement, which is reflected in the ratio ρ_w, is taken into account. The residual shear strength, V_{res}, of the given two types of bridge decks due to corrosion can be calculated as:

$$V_{res} = \left[8\lambda_s \lambda \left(\rho_w^* \right)^{1/3} \sqrt{f_c'} + \frac{N_u}{6A_g} \right] b_w d \qquad \text{Equation 2.14}$$

where ρ_w^* is the reinforcement ratio with the corroded longitudinal rebars, and f_c' is the compressive strength of the concrete in the web region of the cross-section. In the literature, several researchers, such as Azam and Soudki (2012), El-Sayed (2017), El-Sayed et al. (2016), Frontera and Cladera (2022), Fu et al. (2023), Han et al. (2019), Juarez et al. (2011), Lachemi et al. (2014), Xue et al. (2014), and Ye et al. (2018), have used Equation 2.14 to determine the shear strength of corroded reinforced concrete beams with no stirrups, and reported conservative predictions of residual shear strength (Han et al., 2020; Tan & Kien, 2021).

2.2.2.2 Contribution from the Stirrups in T-Beam Bridges. In T-beam bridges and one-way slab continuous bridges with stirrups where shear reinforcement is provided in the longitudinal beams running along the deck, and the deterioration of the stirrups due to corrosion is considered in the modeling. The effect of this deterioration is reflected in V_s in the form of the remaining cross-sectional area of the stirrups and the residual yield strength of the corroded stirrups. The residual shear strength of the reinforced concrete bridge with at least minimum amount of shear reinforcement can thus be calculated as:

$$V_{res} = V_{c,res} + \frac{A_v^* f_{v,y}^* d}{s} \qquad \text{Equation 2.15}$$

where $V_{c,res}$ is the residual shear strength contribution from concrete calculated using Equation a or b from Table 2.1, and tuning the parameters ρ_w and f_c' to reflect the corrosion damage as explained earlier; A_v^* s the reduced cross-sectional area of stirrups, which can be calculated using Equation 2.2; and $f_{v,y}^*$ is the residual yield strength of stirrup reinforcement calculated similarly using Equation 2.1.

2.3 Impact of Corrosion on the Structural Performance of Interventions

In this section we discuss the effect of interventions on the degraded structural performance. Since thin deck overlays are applied within the concrete cover, no modifications to the previously derived strength equations are required. Patches, on the other hand, influence the structural model formulation. Their effect on the flexural performance of a non-corroded reinforced concrete cross-section is addressed here using a model developed for that purpose. It is important to note that structural strength is directly affected by how the interventions modify the material degradation process. Therefore, only interventions that modify the mechanical model formulation are presented below.

Patches always improve the strength of a reinforced concrete cross-section from its existing condition. Applying a patch will remove all corrosion cracks, effectively setting the crack width in the section to zero. It can also improve the cracking resistance of the section as well as the bond strength of the rebar. Depending on the properties of the patch, it can act as a corrosion inhibitor as well. This behavior makes patches essential for both positive and negative moment regions.

In the tension region, the strength contribution from the concrete is ignored, thus, the patching in this region affects the tension bars only. The yield strength of the rebar is unaffected by the change in the material around it. The bond strength of the bar is influenced by the change of material properties around the rebars. The development length of the rebar depends on the yield strength of the rebar and the tensile strength of the concrete surrounding it. The development length of the rebar is inversely proportional to the tensile strength in terms of the square root of the compressive strength of the concrete surrounding it. Hence, less development length would be required by rebars with an increase in the tensile strength of the material surrounding it in the case of a splitting bond failure. Since the material used for patching is expected to have a strength greater than or equal to the strength of the concrete substrate, the development length required to yield the bars is expected to be reduced. Moreover, from Equation 2.3 we can observe that the bond strength of the rebar is expected to improve as it is directly proportional to the strength of the material surrounding it (Vembu & Ammasi, 2023). To understand the effect of patching on the tension force in the rebars due to bond stress, consider Figure 2.2 and the discussion that follows.

Let the length of the patch be l_p and the development length of the rebars be l_d such that the development length of the rebars is greater than the patch length. For a section AA' at the middle of the patch, we can observe that the bond stress changes media from the patching material to the concrete substrate, as depicted

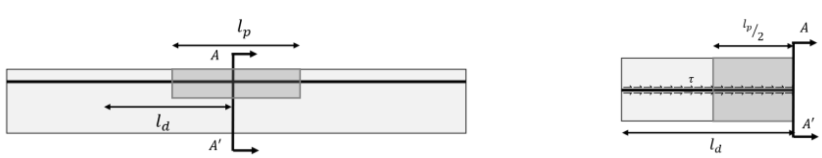

(a) Elevation view of a negative moment region of a continuous reinforced concrete bridge deck with patching in tension region.

(b) Influence of patching on the bond stress of tension rebars.

Figure 2.2 Effect of Patching on the Stresses of a Reinforced Concrete Member.

in Figure 2.2b. The force in the tension rebars due to bond stress can be calculated as:

$$T_{bond} = \int_0^{l_d} \tau \ \pi \ d_b \ dx = \int_0^{l_p/2} \tau_{rep} \ \pi \ d_b \ dx + \int_{l_p/2}^{l_d} \tau_{sub} \ \pi \ d_b \ dx$$

Equation 2.16

where τ_{rep} is the bond stress in the patch, and τ_{sub} is the bond stress in the concrete substrate. We can observe that the bond force would also improve with a higher strength of the patching material. Section AA' would have a higher bond force as it covers the maximum length of patching material. For sections other than AA' within the patch, the distance closer to the substrate boundary should be considered while calculating the bond force. This improvement in bond force would improve the cracking resistance of the section and delay the yielding of the rebars. This phenomenon is reflected in the results of Saifullah et al. (2023).

2.4 Influence of Interventions on Corrosion

Besides structural performance, interventions influence the corrosion process. When properly implemented, interventions slow or even halt some of the deterioration mechanisms. In this subsection, we describe the effects of intervention on the chloride penetration and the rust expansion stages of the corrosion process.

Before the intervention, the chloride penetration in the structure is governed by the diffusion of ions through concrete and characterized through a single diffusion coefficient that determines the pace at which the chlorides penetrate the concrete. A typical original section, that is, a section without interventions, is shown in Figure 2.3a. When a thin deck overlay is applied, the chlorides must flow through three layers: the thin deck overlay, the patched region (if any), and the pre-existing or substrate concrete. As indicated in Subsection 2.1.1, the thickness of the thin deck overlay is typically an approximate 3/8 in. (9.53 mm) thick. The shot blasting depth is usually ¼ in., which leaves a thickness of the added epoxy material of approximately ⅛ in. In the case of a rigid deck overlay, the milling varies from ¼ to ½ in. from the surface of the deck. If a patch is needed in either of these two cases, that is, when placing a thin or a rigid overlay, the patching depth will depend on the soundness of the concrete. In the most critical cases, the weak concrete will reach down to the rebar. For exposed bars, INDOT requires removing 1 in. of concrete below the rebar (INDOT, 2022b). Figure 2.3b and Figure 2.3c show sections intervened with thin and rigid deck overlays, respectively. In both cases, we also indicate the critical patching depth of 1 in. below the rebar.

In general, each layer is characterized by a different diffusion coefficient. In other words, the pace of chloride penetration is different for each layer depending on the age and amount of cracking of the respective layer. The diffusion coefficient increases with cracking and decreases with age. Note that the depth of the entire concrete section is larger after the thin deck overlay application due to the addition of the epoxy material and crushed limestone on the top of the deck.

Regarding rust expansion, in the sound section, the critical rust pressure is a function of the cover thickness, the tensile strength of the concrete, and the rebar diameter. According to Kim et al. (2016), the critical rust pressure needed to crack the concrete can be up to 80% less in a patched section when compared to a sound section, which can be explained by the reduced strength at the joint between the substrate and patching material.

3. VOIDS ON CONCRETE DECKS AND SLABS

3.1 Definitions

Several terms are used to describe the presence of air voids in concrete, both in the specialized literature and in civil engineering practice. However, not all these terms describe the same phenomenon. Indeed, not all the described phenomena are prejudicial to the performance of the structure. In this section, relevant concepts are described that involve air voids in concrete decks, one-way slabs, and T-beam bridges, as well as commonly used terms.

Cement is a material with a porous nature that will inevitably contain air voids. ACI (2013) defines the term *air voids* as any space in cement paste, mortar, or concrete that is filled with air. The *air content* is the measure of the volume of voids in the mix and is usually expressed as a percentage of the total volume of the mix. There are nuances and differences among the air voids depending on size, shape, and intention of inclusion. The smallest air voids of interest from a construction point of view are *capillary voids*, a network of microscopic air bubbles that can

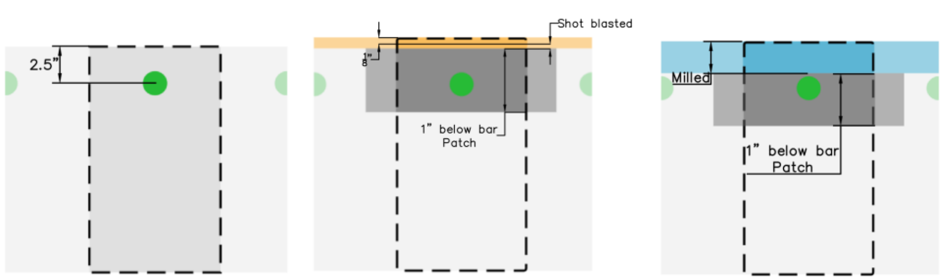

(a) Original Section (b) Thin Deck Overlay (c) Rigid Deck Overlay

Figure 2.3 Different Patching Depths.

range from 0.0004 to 0.002 mil (10 to 50 nm). Capillary voids are mainly dependent on the water-to-cement (w/c) ratio of the cement or mortar paste (Mehta & Monteiro, 2006).

Besides the inherent network of capillaries in the paste, every concrete mix must contain a minimum amount of air to counter the effects of drying shrinkage, creep, and freeze-thaw cycles. This minimum amount of air is both desirable and intentional, that is, it is typically included in the mix design. ACI suggests the term *entrained air* to refer to these microscopic (diameter of 0.004 in. to 0.04 in.; 0.1016 mm to 1.016 mm) and spherical air bubbles intentionally incorporated in the mix using air-entraining agents or admixtures (ACI, 2013). ACI reserves the term *entrapped air* for air voids not included in the design and unintentionally created during the mixing process due to, for example, improper vibration during concrete placement. Opposed to entrained air, the entrapped air bubbles are irregular in shape and usually 0.04 in. or larger in size. Entrapped air bubbles usually emerge as *surface air voids* (informally called "bug holes" in practice), defined by ACI as small regular or irregular cavities, typically less than 5/8 in. (15.875 mm) in diameter, that appear in the surface of formed concrete during placement and consolidation. Entrapped air bubbles can also stay in the interior of the cast concrete after hardening, thus creating air voids known as *honeycombs* (ACI, 2013). Honeycombs are air gaps within the concrete resulting from the segregation of the coarse aggregates from the fine aggregates and the cement paste (Ryan et al., 2023).

From the definitions introduced above, we can conclude that entrapped air, which leads to surface air voids and honeycombs, is a pathological form of air intrusion not considered in the mix design. Thus, entrapped air voids and their two outcomes, surface air voids and honeycombs, are the focus of this work. Unless specified otherwise, the terms entrapped air voids and voids will be used interchangeably.

3.2 Sources of Voids

In the field during construction, voids and other defects can arise due to improper construction practices. Here is a summary of improper construction practices leading to voids collected after interviewing INDOT Research Division personnel.

- **Improper Placement of Bar Supports (Chairs):** Chairs are used for supporting the reinforcement in concrete decks. These chairs are 1.5 in. (38.1 mm) in height; hence, the bottom reinforcement is placed at a distance of 1.5 in. from the formwork. The problem with this is that the chairs are too close to the formwork. The maximum aggregate size specified in INDOT bridge deck mixes is 1 in., and as per ACI requirement, for the free flow of aggregates from side to side through the chair, the spacing from the formwork to the bottom reinforcement should be three times the maximum aggregate size, or 3 in. (76.2 mm). When the available spacing is only 1.5 in. (38.1 mm), this may lead to honeycombing at the bottom of the deck.
- **Improper Consolidation of Concrete:** Contractors must properly vibrate the concrete so that the aggregate can go through the chair. A Spud Vibrator should be used to perform the vibration every foot to avoid aggregate segregation, which leads to honeycombs at the bottom of the deck. An incorrect vibration technique, especially when the space between the bar and formwork bottom is tight, may increase the incidence of honeycombing in the concrete bridge deck. A combination of a Form Vibrator, to vibrate the bottom, and a Spud Vibrator, to consolidate the top, is recommended for slab bridges to avoid honeycombing. Honeycombs are observed only after construction since formwork is present at the bottom during the construction. They would not be visible if stay-in-place deck forming is used. Honeycombing can also occur close to the top of the deck if the contractors are not careful and may not be visible. In such situations, Impact Echo (IE) or Ground-Penetrating Radar (GPR) may be used to identify honeycombs.
- **Concrete Mix:** The other cause of honeycombing is improper slump of the concrete. The ideal slump required by INDOT is 2–6 in. (101.6–177.8 mm; INDOT, 2022b). But if the contractor does not meet this slump requirement which, according to the interviewed INDOT's Research Division personnel, is very rare, then honeycombs are likely to form, which can even cause air to be entrapped in the concrete. Honeycombs present at the midspan of the bridge are the most concerning. Their presence reduces the concrete strength and increases the possibility of surface cracking where they appear.
- **Improper Aggregate Gradation:** A coarse mix, that is, a concrete mix with an excessive quantity of coarse aggregates, produces a lot of air bubbles, while a fine mix, that is, a concrete mix with an excessive quantity of fine aggregates, may not produce any air bubbles at all. The ideal mix design falls in between a coarse mix and a fine mix such that minimum voids are present in the sample, it contains the required proportions of all standard fractions of aggregates (Shetty & Jain, 2019).
- **Improper Mixing:** Entrained air in concrete helps protect it against freeze and thaw cycles. Entrapped air, which is larger in size than entrained air, is formed when concrete is not mixed properly for enough time. INDOT's *Standard and Specifications* (2022b) specify that the concrete should be mixed for at least 60 s in a stationary mixer. The drum's rotation speed shall be in the range of 14 to 20 revolutions per minute. In the case when concrete is not sufficiently mixed, it eventually forms large voids, even if the slump requirement is met. Incorrect dosage of air-entraining admixtures and water-reducing admixtures is also a main reason behind the formation of large voids. As the size of air voids in concrete increases, the compressive strength of the concrete is reduced. The acceptable range of air voids is 5–8%.

Improper construction practices in screeding and the casting sequence can also result in errors associated with the thickness of the concrete deck over girders, one-way slabs, and T-beam bridges.

- **Screed:** Screeding is the leveling operation performed using a roller when the concrete is cast. Improper screeding causes the surface level of the deck to vary, resulting in variation in the overall thickness of the deck.
- **Casting Sequence:** In a reinforced concrete bridge deck on precast or steel girders, the spans are separated by piers and the negative primary tension reinforcement bars providing continuity run over the piers and cross into the adjacent span. When concrete is poured into one span, the reinforcement in the span where the pouring is taking place may move down, while the reinforcement in the adjacent span may rise. This behavior causes the deck thickness to increase at the midspan and to decrease at the top of the piers.

According to the interviewed personnel, the combination of both improper screeding and improper cast sequence can cause errors in the thickness of the deck in almost 50% of the bridge deck area.

3.3 Impact of Voids on the Deterioration Process

Air voids can have detrimental effects on the durability of bridge decks. This section describes the mechanisms by which air voids influence the corrosion-induced deterioration.

3.3.1 Chloride Penetration

The rate at which chlorides move through the concrete cover is determined by the transport properties of concrete. There are three main types of transport phenomena including: advection, diffusion, and electromigration. Here, we focus on advection and diffusion as they are the most common penetration mechanisms in bridge concrete decks. Advection is the process by which ions, carried by water flowing through the cement matrix due to pressure gradients, are transported in concrete. The volumetric flux of water, q, that is, the rate of volume flow across a unit area, is given by Darcy's constitutive equation for isotropic porous media (Mehta & Monteiro, 2006)

$$q = \frac{k}{\mu}\frac{dP}{dx}, \qquad \text{Equation 3.1}$$

where k is the intrinsic permeability of water in concrete, μ s the viscosity of water, and $\frac{dP}{dx}$ is the pressure gradient through a differential distance dx. Multiplying Equation 3.1 times the concentration of ions in the water, C, we obtain the advective mass flow, J_a, in $\mathrm{kg/m^2s}$:

$$J_a = C\frac{k}{\mu}\frac{dP}{dx}. \qquad \text{Equation 3.2}$$

Diffusion is the process by which ions are transported through saturated media due to concentration gradients. Diffusion is governed by Fick's First Law (Claisse, 2021), which gives the diffusive mass flow, J_d:

$$J_d = D\frac{dC}{dx}, \qquad \text{Equation 3.3}$$

where D is the diffusion coefficient in $\mathrm{m^2/sec}$. In general, the concentration, C, in Equation 3.2 and Equation 3.3 vary with the distance x. The rate of change of C is determined by Fick's Second Law (Claisse, 2021):

$$\frac{\partial C}{\partial t} = \frac{\partial}{\partial x}\left[D\frac{\partial C}{\partial x}\right]. \qquad \text{Equation 3.4}$$

Equation 3.4 represents the most widely used method to model the penetration of chloride ions in concrete surfaces. Its usage depends on the assumption that the concrete is completely saturated, as is usually the case in the splash zones near coastlines or bridges where deicers have been applied. However, even under these two scenarios, not all regions of the concrete surface saturate. The saturation rate in the concrete is mainly given by the permeability of the concrete, k, and governed by Equation 3.1. Thus, advection and diffusion, as well as their two characterizing parameters, k and D, are closely related. This relationship is evident for gas or vapor movement. In such a case, assuming ideal gas behavior (Claisse, 2021):

$$D = \frac{nRT}{V\mu}k \qquad \text{Equation 3.5}$$

where n is the number of moles of gas, R is the ideal gas constant, T is temperature, and V is volume.

Both D and k depend on the porosity, ε, of the concrete, which is defined by ACI's *Concrete Terminology* (2013) as the ratio of the volume of voids in concrete to the total volume of concrete. This dependency is explicit in, for example, the Kozeny-Carman equation (Kruczek, 2015),

$$k = \frac{M_S^2\varepsilon^3}{\tau\left(1-\varepsilon\right)^2}, \qquad \text{Equation 3.6}$$

or the relation (Ahmad & Azad, 2013)

$$D = \frac{\varepsilon}{\tau}D_0, \qquad \text{Equation 3.7}$$

where M_s is the specific surface area per unit volume of solid material, τ is the tortuosity of the concrete, defined as the squared ratio of the average effective flow path to the shortest length along the major flow axis of the porous medium (Ahmad & Azad, 2013), and D_0 is the pure gas diffusion coefficient.

We can conclude from Equation 3.4 to Equation 3.7 that a higher number of voids lead to a faster chloride penetration. This relation between porosity and transport properties has been experimentally observed by Shafikhani & Chidiac (2019). In a comparative study, they conclude that the most accurate and precise diffusion coefficient models are the ones that account for capillary porosity and pore structure parameters.

Despite the evident relationship between porosity, diffusivity, and permeability, the complex nature of transport phenomena in concrete makes it difficult to establish a corresponding quantitative relationship. For instance, Wong et al. (2011), observed that every 1% increase in air content either increases the transport properties by 10% or decreases them by 4% depending on whether the voids are acting as conductors or insulators. Zhang et al. (2018) reported that a moderate inclusion of air (4% to 5%) lowers ion migration with respect to the case of no air entrainment, whereas a high inclusion of air (7% to 10%) raises ion migration. More experimental research is needed to determine the specific causes of this seemingly inconsistent behavior. For this study, it is assumed that a higher number of voids promotes interconnectivity. In the case with the higher number of voids, which is the case considered in this research, the diffusion coefficient is assumed to increase, as suggested by Equation 3.5 to Equation 3.7.

3.3.2 Chloride Threshold

The amount of accumulated chloride ions that the protective layer of the steel rebar can withstand before depassivation is known as chloride threshold. A low chloride threshold implies earlier corrosion of the rebar. As Bertolini et al. (2003) point out, the chloride threshold depends on the presence of macroscopic voids in the concrete near the steel surface. For example, a reduction in air entrapment from 1.5% to 0.2% increases the chloride threshold from 0.2% to 2% of the mass of cement.

3.3.3 Mechanical Properties

For homogeneous solids, strength and porosity have an inverse relationship (Mehta & Monteiro, 2006):

$$f = f_0 e^{-\kappa\varepsilon}, \qquad \text{Equation 3.8}$$

where f is a generic strength (i.e., it can be either compressive or tensile strength), f_0 is the generic strength at zero porosity, and κ is a constant characteristic of the material. While it is true that concrete is a heterogeneous, multiphase material, the strength-porosity relation given by Equation 3.8 is still because the porosity in each phase of the concrete indeed reduces the strength in that respective strength. That is, a more porous cement matrix has less strength than its idealized non-porous equivalent.

Mehta and Monteiro (2006) discussed the case of compressive strength, f_c. The f_c of a mix with 6% of entrapped air can be 35% of the mix without entrapped air. Zhang et al. (2018) observed the same pattern in a series of experiments with both ordinary Portland cement concrete and concrete with fly ash. For ordinary concrete with a w/c ratio of 0.35, the compressive strength with 10% of entrapped air is 50% of the compressive strength with 3.2% entrapped air. Zhang et al. (2018) studied the reduction in compressive strength for w/c ratios of 0.35 and 0.53 and observed, as Mehta and Monteiro did, that the reduction is more pronounced for concrete with lower w/c. This observation confirms the validity of Equation 3.8, at least from a qualitative standpoint, and will thus be used in this study to model the variation of strength with entrapped air.

The increase in air voids also impacts the elastic modulus, E, and the tensile strength, f_t, of the concrete. This conclusion is evident from the formulas suggested by ACI (ACI Committee 318, 2005a, 2025b) for these two properties, which are dependent on the compressive strength:

$$E = 57000\sqrt{f_c} \ \text{(psi)} \qquad \text{Equation 3.9}$$

$$f_t = 7.5\sqrt{f_c} \ \text{(psi)} \qquad \text{Equation 3.10}$$

with f_c in psi, and

$$E = 4700\sqrt{f_c} \ \text{(MPa)} \qquad \text{Equation 3.11}$$

$$f_t = 0.56\sqrt{f_c} \ \text{(MPa)} \qquad \text{Equation 3.12}$$

with f_c is in MPa.

3.3.4 Cracking

Corrosion is not the only source of cracking in concrete; drying shrinkage, thermal shrinkage, and mechanical fatigue are also common cracking mechanisms both in decks and slabs, and in T-beam bridges (Mehta & Monteiro, 2006). Entrapped air voids are relevant to all these mechanisms. In fact, shrinkage related to differential drying is exacerbated by the presence of air voids. Moreover, large air voids can reduce the ability of the concrete to uniformly conduct heat, causing a differential thermal expansion and contraction that increases the potential for thermal cracking to occur. Finally, the reduction in the tensile strength described in the previous subsection, together with the stress concentration at the edges of surface air voids, creates localized zones with high number of air voids that are susceptible to mechanical fatigue cracking. Shiotani et al. (2003) experimentally observed this correlation between air voids and cracks using optical microscopy.

4. DETERIORATION MODEL

In this section, we provide a description of the model developed to assess the impact of voids on the performance of decks and slabs. First, we summarize an existing corrosion model that captures the most relevant aspects of the corrosion-induced deterioration process. Then, we describe the modifications and extensions made to that baseline model to ensure it is suitable for bridges in Indiana, as well as the inspection and rating abilities added to that model for this project. Finally, we describe the elements of the model that are used to introduce the effect of voids on the lifetime of a deck.

4.1 Baseline Corrosion Model

The corrosion model developed by Papakonstantinou and Shinozuka (2013) is adopted as a baseline for this research (see Figure 4.1). The baseline model is divided into the three stages or phases of the corrosion process: penetration, rust expansion or corrosion development, and cracking. In their approach, Papakonstantinou and Shinozuka modeled individual corroding "cells" that represented a single point in a surface. The boundary conditions between the individual cells were captured by introducing correlated parameters along a surface composed of several individual cells. The top and bottom of a single cell correspond to the top and bottom of a deck, respectively. A deck is thus divided into a group of finite-area cells. For this project, we focus on a finite strip of the bridge and consider it representative of the entire deck. Specifically, for the illustrative case study of 6, we will focus on the modeling of a longitudinal section of the bridge.

A summary of the notional baseline model and its relevant inputs appear in the diagram of Figure 4.1, which is explained as follows. For each individual cell, the penetration phase is modeled using Fick's Second Law of diffusion (Equation 3.4). The main parameters or inputs of the penetration phase are: (1) the diffusion coefficient, which dictates how fast the chlorides penetrate; (2) the chloride concentration at the top of the cell, that is, at the top of the deck, hereafter referred to as surface chloride concentration; (3) the concrete cover of the rebar; and (4) the critical chloride concentration, or chloride threshold, needed for the corrosion process to start.

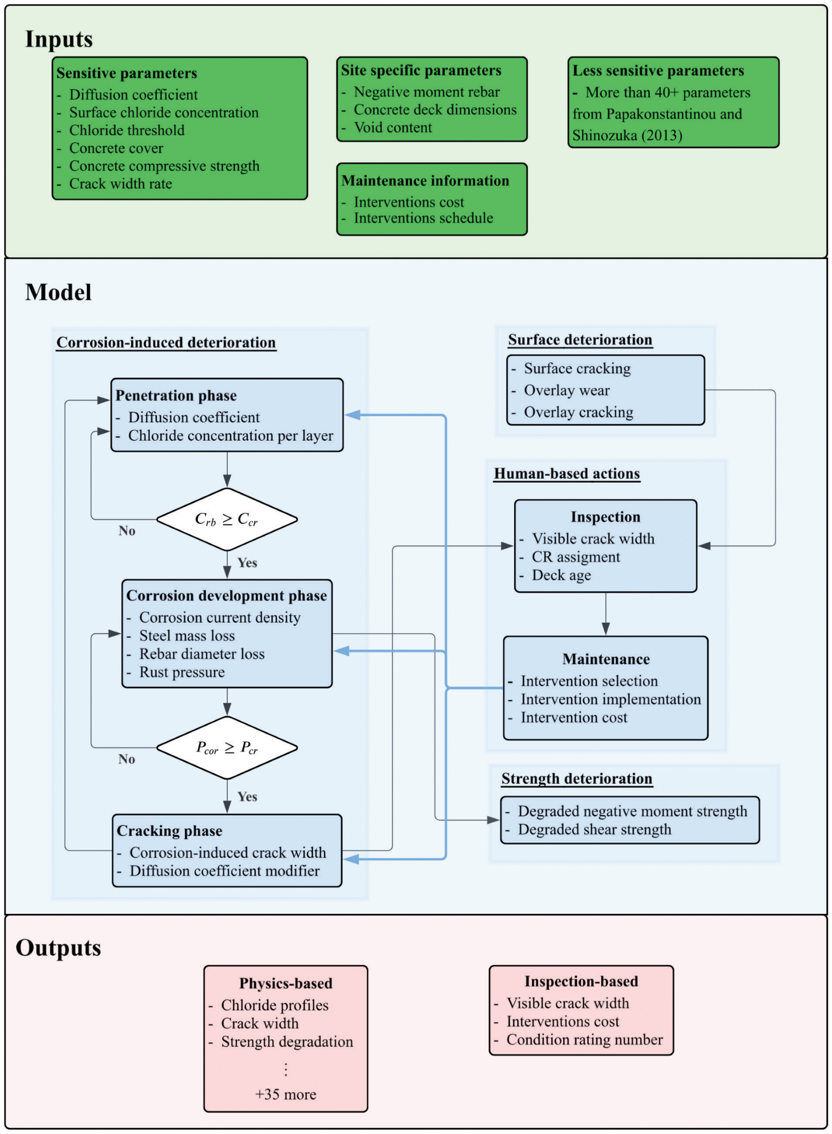

Figure 4.1 Diagram of the Deterioration Model Used for This Project.

The corrosion starts when the chloride concentration at the rebar level exceeds the chloride threshold. Then, the corrosion development phase is described by a corrosion current density caused by the electrochemical nature of the corrosion process. Corrosion degrades the rebar, reducing its mass and, consequently, diameter. The mass that is lost due corrosion accumulates as a rust by-product at the interface between the rebar and the concrete. When the pressure exerted by the rust is larger than a critical threshold, the concrete cracks. During the cracking phase, the crack resulting from the rust pressure accumulation keeps widening. The faster and higher the corrosion process is, the faster and wider the crack will open. Moreover, the more cracking the concrete has, the faster the chlorides will penetrate and accelerate the corrosion process. This feedback between cracking and penetration is modeled by a diffusion coefficient modifier.

4.2 Deterioration Model for Bridge Decks and Slabs

The baseline model shown in the left portion of Figure 4.1 was developed by Papakonstantinou and Shinozuka (2013) to analyze corrosion in maritime environments. Thus, it does not capture phenomena that are critical for bridge decks and slabs. For example, bridge condition rating numbers depend not only on the corrosion-induced cracking, which initially occurs between 10 and 12 years of the lifetime of a bridge deck, but also on the fatigue or shrinkage cracking that start developing shortly after construction and independently from the corrosion process. In a previous JTRP project (SPR-4526 from Criner et al., 2023), this type of cracking was represented using a linear model. Details on the implementation of this model can be found in Salmeron et al. (2024). Here, the cracking occurring at the surface of the deck, hereafter referred to as surface cracking and denoted $\omega_i(t)$, is modeled using a saturating function:

$$\omega_i(t) = m_w \cdot \tanh^{-1}\left(\frac{k_w}{t}\right) \qquad \text{Equation 4.1}$$

where the cracking rate constant m_w dictates how fast the surface crack develops, and the time constant k_w controls the time where the crack reaches its maximum value.

To link this empirical cracking rate to physical principles, we can relate it to the physics-based Griffith law for cracking:

$$\sigma = \sqrt{\frac{2E\gamma}{\pi a}}, \qquad \text{Equation 4.2}$$

where E and γ are the elastic modulus and the surface energy density of concrete, and a is half of the length of the crack. We aim to obtain a qualitative relationship between Griffith's law and our defined cracking rate m_w. We must note that the relationship we intend to obtain is empirical or heuristic and does not constitute a formal mechanics formulation. Assuming that the stress at which the cracking of concrete in the surface happens is the tensile strength, f_t, we can set $\sigma = f_t$. Clearing a from (28) and taking its time derivative, we obtain:

$$\dot{a} = -\frac{2E\gamma}{\pi f_t^3}\dot{f}_t, \qquad \text{Equation 4.3}$$

which has the same units as m_w, that is, depth (or width) per time. We can assume that the rate of change of f_t, $\dot{f}_t$, is negative, because although strength increases over time, freeze-thaw cycles and cracking are more impactful after the curing time (28 days) has been reached. Thus, regrouping terms:

$$m_w = \left(\frac{2|\dot{\sigma}|\gamma}{\pi}\right)\frac{E}{f_t^3} = b\frac{E}{\sigma^3} = b\frac{4700\sqrt{f'c}}{0.56^3\left(f'c\right)^{3/2}} = b\frac{4700}{0.1756f'c}$$

which may be rearranged to obtain b:

$$b = \frac{0.1756 \cdot f'c \cdot m_w}{4700} \qquad \text{Equation 4.4}$$

Finally, we can define a heuristic relationship between the surface cracking rate and the mechanical properties of the concrete:

$$m_w = b\frac{E}{f_t^3} \qquad \text{Equation 4.5}$$

The heuristic relation of Equation 4.5 serves as a quick way to model the development and growth of surface cracking in a deck using minimum information. For example, some authors recommend 0.1 mm as a limit value at service loads in severe environments (Mindess et al., 2003). Different values of m_w can be obtained using this limit state and knowing the time at which it should be reached, which can be obtained from experienced inspectors or other sources.

Another aspect incumbent to this work that is not captured by the original baseline model is interventions. In this work, we represent each intervention using multilayered diffusion processes (Hickson et al., 2011), where the diffusion through each layer of the intervened section has a different diffusion coefficient. The different layers corresponding to each intervention stage of the deck and illustrated in Figure 2.3, are briefly summarized as:

1. Original deck: single layer corresponding to the substrate material.
2. Thin deck overlay:
    a. Without patch: two layers corresponding to the thin overlay thickness above the shot blasting depth and the original concrete below.
    b. With patch: three layers corresponding to the overlay thickness on top, then the patching material, and finally the original concrete at the bottom.
3. Rigid deck overlay:
    a. Without patch: two layers corresponding to the rigid overlay thickness above the milling depth and the original concrete below.
    b. With patch: three layers corresponding to the rigid overlay thickness, the patch depth and the original concrete below.

Our model also captures the case where a patch is applied over an existing patch. In such a situation, the number of layers is increased by one. For example, if a patch already exists in an already patched point before applying a rigid deck overlay, and the new patch requires a smaller depth than the existing patch, case 3b above will have four layers: the new patch, the old patch, the rigid deck overlay, and the original concrete.

The expanded version of the deterioration model also includes the effect of overlay wear. The thickness of the overlay at year t, $X_{ovr}(t)$, is computed as (Sancharoen et al., 2008):

$$X_{ovr}(t) = X_{ovr}(0) \cdot \left(2 - e^{a_{ovr}t}\right) \qquad \text{Equation 4.6}$$

where the total wear of the overlay depends on the parameter a_{ovr}. A reduction in the overlay thickness results in a less-effective protection against the ingress of chlorides.

4.3 Spatial Variability

In the previous JTRP project (SPR-4526 from Criner et al., 2023), life and cost quantification analyses were performed under the conservative assumption that a single cell model, that is, a finite, small portion of the deck's surface, was representative of an entire deck. However, some important quantities in the lifecycle of a bridge depend on spatial variations. For example, condition rating numbers and patching cannot be properly characterized assuming a single cell model. Thus, for this project, we implement a strip model that accounts for the deterioration along the length of a deck or slab. Similar to the baseline model described in Section 4.1, we simulate several independent cells whose behavior is correlated through the values of their parameters. The spatial variability between a parameter in a cell and its two neighboring cells is determined, besides the usual probability distribution, by a power spectrum. A general description of these techniques are available in the literature (for example, see Botte et al., 2025).

4.4 Inspection, Rating, and Intervention Scheduling

Extending the model from a single corroding cell to a strip of the deck enables the capturing of features that depend on the length of the deck. For instance, the developed deterioration model includes inspections, assignment of condition rating numbers, and scheduled and condition-based intervention actions. We modeled an inspection occurring at a time T_{ins} defining a visible width at one of the cells of the deck as:

$$\omega_{vis}(T_{ins}) = \max\{\omega_i(T_{ins}),\ \omega_c(T_{ins})\} \qquad \text{Equation 4.7}$$

where ω_i is the surface cracking defined in Section 4.2, ω_c is the corrosion-induced cracking in the cell, and T_{ins} is the inspection time. Both ω_i and ω_c are outputs of the model described in Sections 4.1 and 4.2. For example, if at the time of the inspection corrosion has not cracked the concrete, then the surface cracking determines the value of the visible crack. We must note that, during inspection, it is challenging to differentiate a corrosion crack from a crack occurring due to other phenomena, such as shrinkage or fatigue. For modeling purposes, we assume that these two types of cracks are clearly differentiated.

The visible cracking is used to assign a condition rating number following INDOT's *Bridge Inspection Manual* (2022a), where both crack width and crack spacing are considered as shown in Table 4.1. For assigning a condition rating, the visible cracks of each of the points in the deck are computed using Equation 4.7. Then, the maximum cracks and their spacing are determined. Finally, a condition rating number is assigned using the criteria established in Table 4.1. We must note that delamination and spalling are out of the scope of this project, and thus not considered in the current model for condition rating assignment.

Note that, for the purpose of this project and in the illustrative case study, the rules for condition rating in Table 4.1 are strictly applied.

The model can trigger interventions depending on three factors: (i) the surface and corrosion-induced cracks, (ii) the condition rating number of the deck, and (iii) the age of the deck. Hereafter, the interventions applied as a result of crack width and condition rating number are referred to as *state-based interventions*, and to the interventions based on the age of the deck as *scheduled interventions*. For example, the model has the capability to trigger a thin deck overlay intervention if any one of the following three conditions hold at the time of inspection:

1. The visible cracking (Equation 4.7) is larger than a threshold value,
2. The condition rating number is less or equal than 7,
3. The bridge has reached an age of 10 years.

Conditions 1 and 2 would generate state-based interventions, whereas Condition 3 would correspond to a scheduled intervention. Ultimately, the amount and extent of interventions determine the maintenance cost, as shown in Figure 4.1.

TABLE 4.1
Condition Rating (CR) Descriptions and Related Crack Width (INDOT, 2020).

CR	Description
9	No significant defects.
8	Hairline cracking less than 0.012 in. nominal width and widely spaced.
7	Cracking less than 0.016 in., widely spaced, and less than 5% delamination.
6	Cracking less than 0.020 in. and nominal center-to-center spacing greater than 10 ft. Delamination less than 10%.
5	Cracking greater than 0.020 in. and less than 0.040 in. nominal width and nominal on center spacing not greater than 10 ft. Delamination less than 20%.
4	Cracking greater than 0.040 in. nominal width and nominal on center crack spacing less than 10 ft. Delamination greater than 20%. Unpatched or unsound patching, or spalled areas, visible intermittently.

Conversion factor to metric: 1 in. = 25.4 mm.

4.5 Modeling of Voids

This project aims to study the cases where voids are harmful, thus the following modeling assumptions for the influence of voids are taken:

I. Voids have a diameter larger than 0.04 in. (1.016 mm).
II. The air content in concrete with voids is larger than the entrained air tolerance.
III. Voids are interconnected in the direction perpendicular to the deck's surface.

Assumption I implies that, whenever present in the simulated deck or slab, voids are entrapped air, that is, a pathological case. Assumption II follows similar reasoning: whenever present in the simulation, the air content is beyond the acceptable level at which it is beneficial (for example, in terms of alleviating shrinkage cracking or freeze-thaw cycles). Assumption III establishes that the simulated voids along the depth of the studied structure form a void network. Here, we describe how Assumptions I to III influence the model described in Sections 4.1 to 4.4.

4.5.1 Chloride Penetration

The diffusion of chloride ions through concrete is modeled using Equation 3.4, with the diffusion coefficient being dependent on the concrete's age and temperature, as well as the crack width. Assumption III indicates that the voids will facilitate the transport of liquid and gases through the void network. This behavior implies a faster diffusion of the chloride ions when the voids are saturated, and a slower diffusion when the voids are not saturated. Both effects are simulated through a change in the diffusion coefficient with increasing porosity. Using the simplified Maxwell relation proposed by Wong et al. (2011), and relating it to the saturation of the system, yields

$$D(\varepsilon) = \begin{cases} D\dfrac{1+2\varepsilon}{1-\varepsilon} & \theta \geq \theta_{th} \\ D\dfrac{1-\varepsilon}{1+0.5\varepsilon} & \theta < \theta_{th} \end{cases} \qquad \text{Equation 4.8}$$

where $\theta = V_w/V_v$ is the saturation of water in the voids, that is, the ratio of the volume of water, V_w, to the volume of voids in the concrete, and θ_{th} is the saturation threshold. When the water saturation is above the defined threshold, the diffusion coefficient increases with porosity, and vice versa. Note that $D(\varepsilon)$ reduces to the nominal value of D when $\varepsilon = 0$. Here, we assume the conservative case where the concrete is always saturated, that is, the case $\theta \geq \theta_{th}$ in Equation 4.8.

4.5.2 Chloride Threshold

In the baseline model, the chloride threshold is taken as a normally distributed random variable. The mean and standard deviation are chosen from experimental data published by Kwon et al. (2009). As discussed in Section 3.3.2, a higher porosity translates into a lower chloride threshold.

In the work by Bertolini et al. (2003), it is shown that the chloride threshold is a function of the interfacial voids for different concrete mixes. In this study, we choose a decaying exponential function to characterize this functional relation, given by:

$$C_{th}(\varepsilon) = C_{th0} e^{-\mathcal{C}\varepsilon} \quad \text{Equation 4.9}$$

where C_{th0} is the chloride threshold at $\varepsilon = 0$, and $\mathcal{C}$ is a calibration constant.

4.5.3 Mechanical Properties

We assume that the fundamental inverse relationship between strength and porosity that is explained in Section 3.3.3 holds. To obtain the compressive strength of the concrete:

$$f_c(\varepsilon) = f_{c0} e^{-\kappa\varepsilon}, \quad \text{Equation 4.10}$$

where f_{c0} is the compressive strength of concrete without entrapped air. The elastic modulus and tensile strength of the concrete are then computed using Equation 3.9 and Equation 3.10, and are consequently reduced in the presence of voids. Moreover, the cracking rate m_w, computed using Equation 4.5, increases.

A change in the compressive strength also affects the time to corrosion cracking as follows. In the baseline model, the critical pressure that the concrete can withstand before cracking is given by:

$$P_{cr} = \frac{2X_{cov} f_t}{d_0}, \quad \text{Equation 4.11}$$

which depends on the concrete cover, X_{cov}, the tensile strength of the concrete, f_t, and the diameter of the rebar before corrosion, d_0. Note that a decrease in f_t due to increased porosity leads to a lower critical pressure value, and consequently, to earlier cracking of the concrete.

This decrease in compressive strength also affects the strength of the reinforced concrete section in various ways. First, the bond strength of the rebar would decrease as the initial bond strength, τ_0, is taken as a function of the concrete compressive strength, f_c, as per Equation 2.4. This outcome also decreases the reinforcement strain, ε_s, post-threshold corrosion level as per Equation 2.7 and from strain compatibility, and it decreases the extreme compression fiber strain, ε_{cm}, at the concrete section as well. Further, the decrease in compressive strength would lead to an increase in the neutral axis depth, c as per Equation 2.6. Flexural strength, M_n, is directly related to the concrete compressive strength as given by Equation 2.10 thus, compressive strength would decrease as well. If we combine these individual effects, we observe that decrease in compressive strength f_c due to the increase in porosity has a drastic effect on the residual flexural and shear strength of the reinforced concrete section. It can also result in an increase in deflections and cracking, as both E_c and f_t are taken as a function of the compressive strength of the concrete.

5. GATHERING AND PROCESSING DATA

The deterioration model presented in Chapter 4 has several parameters and variables. Ideally, all these values would be obtained from real field data and/or experiments in the laboratory. However, given the size of the bridge network of Indiana, this would be impractical. Therefore, initially it is envisioned to use relevant existing data available either from tests documented in the literature, bridge drawings, or previously collected by INDOT during inspections to obtain the variability of key parameters. For the deterioration processes considered in this project, a sensitivity analysis performed on a single-cell, no-interventions version of the model indicated that the concrete cover and the diffusion coefficient are the most critical values contributing to the variance of the time to initiation, other sources of information can be leveraged to improve the corrosion model. For this project, chloride concentration profiles and temperature fluctuations were also calibrated using existing data. The following subsections summarize the information on data collected and used for calibration of models.

5.1 Experimental Determination of Diffusion Coefficients

To improve the estimation of corrosion degradation with respect to the presence of chlorides, the diffusion coefficient of concrete INDOT Type C with entrapped-air-induced voids, as well as the diffusion coefficient at the cold joint formed by patching the concrete deck, were investigated experimentally. Entrapped-air voids mainly caused by inadequate compaction in their effect on the concrete durability and strength were also experimentally investigated. This research was needed to validate the effects of voids and patching on the durability of the concrete deck. The initial hypothesis in the experimental program is that the diffusion coefficient will increase as the volume of voids increases. The presence of a cold joint was studied to determine its effect on the diffusion coefficient used in modeling the "intervention" case.

To fulfill the stated objective and verify our hypothesis, standard T 357: *Predicting Chloride Penetration of Hydraulic Cement Concrete by the Rapid Migration Procedure* (AASHTO, 2022) is used, utilizing the cells from standard T 277: *Standard Method of Test for Rapid Determination of the Chloride Permeability of Concrete* (AASHTO, 2023). In addition, the diffusion coefficient was estimated using standard

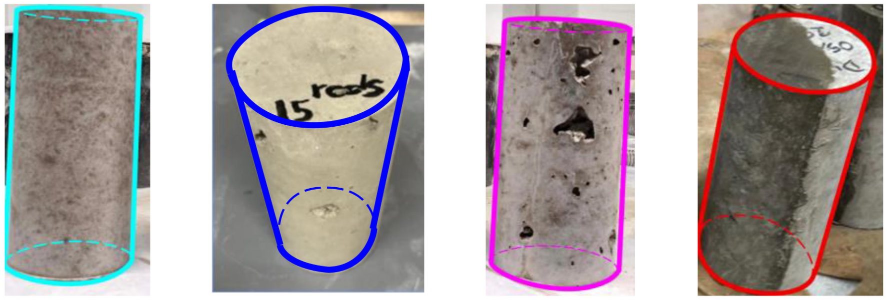

Figure 5.1 Left to Right: 25 Rods, 15 Rods, 5 Rods, and Intervention Cylinders.

Build 492: *Chloride Migration Coefficient from Non-Steady-State Migration Experiments* (Nordtest, 1999).

In addition, to validate the relationship between air void content and diffusion coefficient, the first is determined in fresh concrete using standards ASTM C231: Standard Test Method for Air Content of Freshly Mixed Concrete by the Pressure Method (ASTM, 2022), ASTM C138: Standard Test Method for Density (Unit Weight), Yield, and Air Content (Gravimetric) of Concrete (ASTM, 2024a), and the hardened concrete is determined according to ASTM C457: Standard Test Method for Microscopical Determination of Parameters of the Air-Void System in Hardened Concrete (ASTM, 2024b).

To study the effect of entrapped-air voids, different levels of compaction were applied by altering the number of rodding strokes. Three variations were implemented: 25 rods (overly compacted), 15 rods (intermediate compaction), and 5 rods (poorly compacted). For the intervention case, a first-stage concrete sample (25 rods) was cast, after which a longitudinal half was removed and replaced with second-stage concrete (10 rods), simulating the partial-depth replacement typically performed on concrete bridge decks (Figure 5.1).

The results showed the sensitivity of transport properties to sample height, with the top section, typically the most exposed surface in concrete decks, being more vulnerable to chloride ingress for all void contents. An additional hypothesis evaluated in this experimental program was the effect of cold joints in the case of partial depth deck replacement. Here it was hypothesized that the presence of a cold joint would increase the diffusion coefficient in the "intervention" case. The cold joint, left untreated, created a pathway for chloride ions to penetrate the concrete more easily. Extrapolating to real-world conditions, such as concrete deck patching, suggests that transverse sections near the geometric center of a patch are less vulnerable to chloride ingress than those located near the perimeter. Without specialized treatment, the perimeter may provide an easier pathway for chlorides, increasing the risk of degradation.

5.1.1 Probability Distribution of the Experimentally-Obtained Diffusion Coefficients

We estimated probability distributions for certain model parameters based on our experimental results. Figure 5.2 shows the fitted distributions alongside the normalized experimental data for the top and bottom layers separately. Visually, Figure 5.2 shows that the rank-regression method fits the data slightly better than the Maximum Likelihood Estimator (MLE) method. We thus chose the distributions fitted using rank-regression. Figure 5.2 shows that, for the top layer, the highest median value corresponds to the distribution of the intervention case, while for the bottom layer, the highest median value corresponds to the distribution of the 5 rods case.

We concluded that, for the experiments performed here, the diffusion coefficient values in the top layers of the concrete are the most sensitive to the effect of interventions, while the presence of voids is more impactful in the deeper layers. However, more research is needed to determine if this pattern, observed in concrete cylinder samples, can be extrapolated to bridge decks.

5.2 Modeling Concrete Cover Thickness Using Field Data

The thickness of the concrete cover in a deck is generally considered to be the most effective defense against corrosion. The concrete cover protects the rebar from the harmful environment, namely, chloride ions or CO_2. Moreover, increasing the thickness of the concrete cover enhances the concrete's ability to protect the reinforcement, thereby reducing the likelihood of cracking from the accumulation of corrosion products (Mindess et al., 2003).

Each deck must comply with a prescribed concrete cover defined in the design specifications, which aims to ensure durability. For example, in Indiana, the specification is a 2.5 in. minimum cover to the surface of the reinforcement. However, the pouring of concrete is a highly variable process that hardly guarantees a constant, uniform value over an entire deck. Thus, it is normal to see fluctuations from one point of the deck to another. Several authors have attempted to capture the randomness of the concrete cover. For example, Kirkpatrick et al. (2002) and Kwon et al. (2009) modeled the variability of the cover as a random variable with a normal distribution. Papakonstantinou and Shinozuka (2013) implemented a correlated random field with a Rice distribution to avoid negative cover values. In the absence of correlation data, they also proposed a correlation function based on engineering criteria.

The working dataset includes GPR data collected from 31 bridges. GPR data is collected by rolling a GPR unit in straight lines along a bridge deck. The unit logs the time required

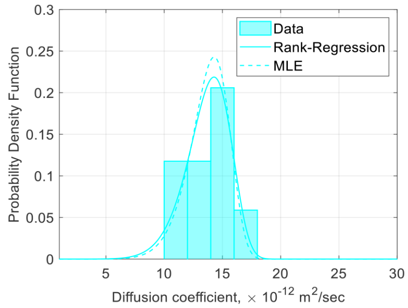

(a) 25 Rods, Top Layer

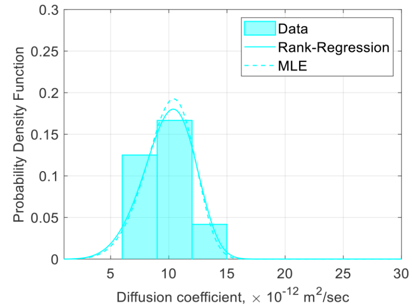

(b) 25 Rods, Bottom Layer

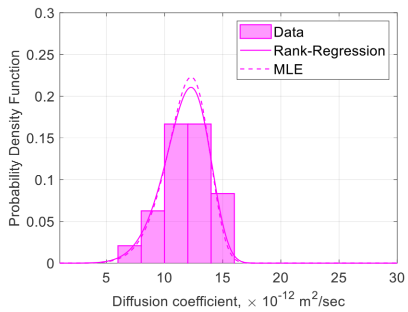

(c)5 Rods, Top Layer

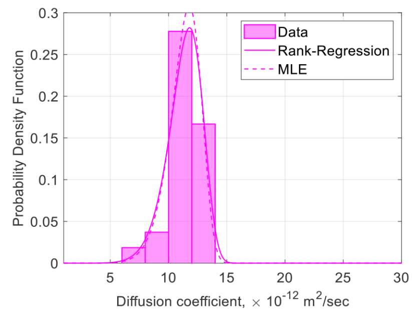

(d) 5 Rods, Bottom Layer

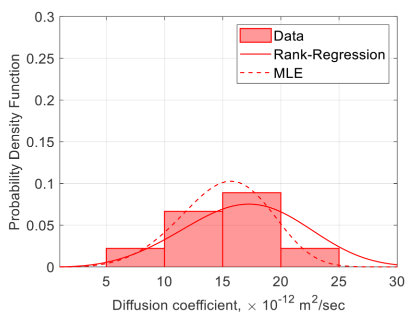

(e) Intervention, Top Layer

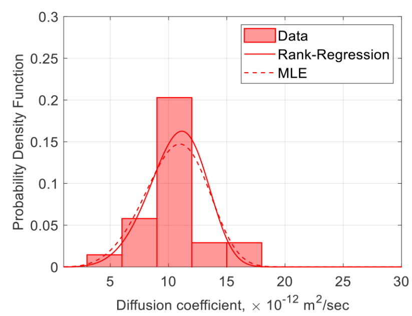

(f) Intervention, Bottom Layer

Figure 5.2 Fitted Weibull Distributions Plotted Alongside the Experimentally Obtained Diffusion Coefficients.

for electromagnetic waves to reach and then reflect from below-surface objects. Those objects primarily would include the steel rebar or the bottom of the slab. The measured signal is registered as both the travel time and wave amplitude along each pass of the GPR unit. The goal of this analysis was to determine the variability in the concrete cover to calibrate this parameter in the model developed.

We processed the data to retrieve the measured cover over the rebar. The first step is to convert travel time, T, into distance, x, using the following equation (U.S. Environmental Protection Agency, n.d.):

$$x = \frac{11.8}{2\sqrt{c_p}} T \qquad \text{Equation 5.1}$$

where c_p is the permittivity of concrete and varies from 8 to 12 in saturated concrete. These data can be visualized in two ways: A-scans and B-scans. An A-scan shows objects (indicated by a rise in amplitude) at one point along the GPR the path of a unit, creating a one-dimensional (1D) visual. A B-scan combines a strip of A-scans into a two-dimensional (2D) representation, illustrating a sort of map of the subsurface objects along the path that the GPR unit took during data collection. The data collected from each of the 31 bridges in our dataset has about 14,000 data points, corresponding to locations where rebar has been located. We grouped these points into strips, or A-scans, and estimated their probability distribution and power spectral density to characterize the spatial variability of the concrete cover.

We found that the best model for the distribution of most A-scans in the GPR data were a lognormal probability distribution with location and scale parameters of 0.0903 and 0.0889, respectively, with an Akaike Information Criterium of -578.32

and passing the Kolgomorov-Smirnov test at a 95% confidence level. The best fit for the spectrum was an exponential spectrum with correlation length of 3.61 ft, with an $R^2 = 0.95$ and root-mean square error of 0.003 with respect to the experimental spectrum.

5.3 Surface Chloride Concentration Using Field Data

To characterize the chloride concentration, we were provided with a data set of chloride concentration profiles from 20 bridges using hammer drill tests. The tests were performed between 1990 and 2001. However, not all the bridges were tested in the same years, nor were the same number of samples obtained from each of the bridges.

The deterioration model developed for this project requires chloride concentration at the surface level as an input parameter. Several authors treat chloride concentration at the surface as a value that remains constant over time (Kwon et al., 2009; Papakonstantinou & Shinozuka, 2013). However, it has been shown that the chloride concentration at the surface level is time-varying and its magnitude influences the time to initiation. For instance, Kassir and Ghosn (2002) used data from 15 different decks in Washington, Minnesota, Pennsylvania, Maryland, and New York to fit the exponential model:

$$C_s\left(t\right) = C_0\left(1 - e^{-\alpha t}\right), \qquad \text{Equation 5.2}$$

which complies with the chemical notion that a surface will saturate with chlorides over time. For their dataset, the authors obtained values of 9 lb/yd³ for C_0, and 0.25 year-1 for α, with a coefficient of determination $R^2 = 0.62$.

Here, we adopt the same approach as Kassir and Ghosn (2002). However, the time span of the data set in this project is significantly shorter than theirs, which constituted biennial measurements over a period of 15 years. Moreover, some of the bridges in our data set likely received an overlay in between measurements. These interventions are not always reflected in the inspection and maintenance histories given in the INDOT database, iTAMS. Nonetheless, a change in the surface concentration from a higher value to a lower value from one year to another is indicative of the existence of treatment during the corresponding period.

In addition to fitting the parameters to the data, we fitted a probability distribution to the data. Using a probability distribution is the best approach to incorporate these parameters in the stochastic model that we will use to assess the lifecycle of the deck. To fit probability distributions, we used the bootstrap method with 1000 samples. We assessed the fit of several possible skewed distributions: lognormal, gamma, Weibull, and inverse Gaussian. All of them have positive support, which guarantees that the parameters will be positive and thus will comply with the physical constraint of chloride accumulation being strictly positive. We computed AIC each case to determine the distribution with the best fit. The lognormal distribution produced the least AIC for both cases. Thus, we chose it as the best fit for each parameter: for C_0, with $\mu = 2.8041$ and $\sigma = 0.0789$; for α, $\mu = -1.0466$ and $\sigma = 0.1626$. Figure 5.3 shows the probability density functions fitted to the bootstrap samples of each parameter.

5.4 Temperature Fluctuations

Temperature variations affect the magnitude of the diffusion coefficient, thereby influencing the process of chloride penetration (Papakonstantinou & Shinozuka, 2013; Salmeron et al., 2024). We selected one of the meteorological stations in the northern part of Indiana (41°00’ N, 87°30’) as our data source. We retrieved surface temperature data from the MERRA–2 database maintained by NASA (Global Modeling and Assimilation Office, n.d.) for the meteorological station in the chosen location. We followed the similar approach to that described for the surface chloride concentration. We chose as a candidate model the sinusoidal given by:

$$T\left(t\right) = A\sin\left(2\pi ft + \phi\right) + C_0 + Ct. \qquad \text{Equation 5.3}$$

The values obtained for the parameters are $A = 13.88°C$ $f = 1$ yr⁻¹, $\phi = 4.65$ rad, $C_0 = 9.50°C$ and $C = 0.04°C \cdot$yr⁻¹. We obtained a coefficient of determination of $R^2 = 0.96$ for the fitted model. The data alongside the fitted model appear in Figure 5.4.

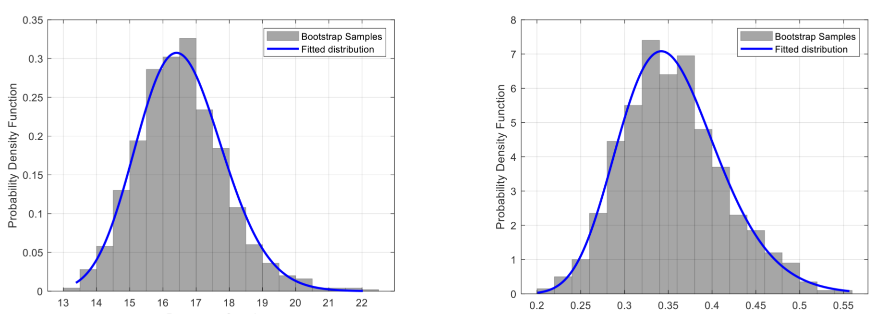

(a) Parameter C_0 (b) Parameter α

Figure 5.3 Probability Density Functions of the Fitted Distributions Alongside the Bootstrap Samples.

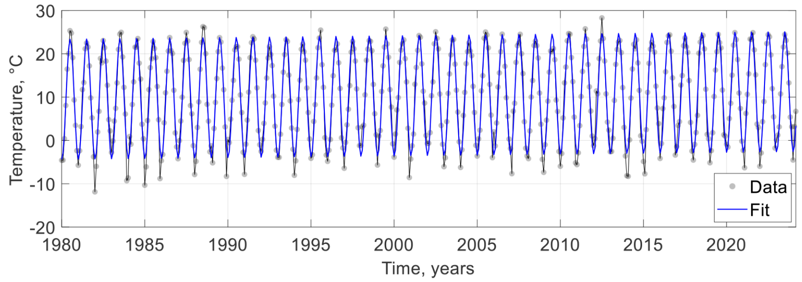

Figure 5.4 Temperature Data and Fitted Model.

6. ILLUSTRATIVE CASE STUDY

In this section the application of the models developed in this project is illustrated on a specific bridge. In this case study, the impact of an excessive number of voids within the thickness of the deck is of interest. Moreover, we conservatively assume voids of size larger than 0.04 in. (1.016 mm) visible at the surface of the deck. The intention is to assess their effect on the service life of the bridge and, consequently, on long-term costs. The costs are assessed not in absolute terms, but relative to a bridge with void content and maximum size that fall within the specification values (INDOT, 2022b).

The asset selected in concurrence with the Study Advisory Committee is 030-43-04852 CEBL, a continuous three-span reinforced concrete solid slab bridge. According to the iTAMS database, the original drawings for this bridge go back to 1964. Over its lifetime, the deck experienced significant chloride-induced deterioration and was ultimately replaced in 2022, resulting in more than a 50-year service life. The replacement bridge superstructure, shown in Figure 6.1, exhibited an unexpectedly high number of voids in the slab.

6.1 Input Parameters

The assumptions of the deterioration model were defined in Section 4. The statistical models of the most relevant parameters of the model are summarized in Table 6.1 below. We report the mean, standard deviation, and correlation lengths. Correlation length is the distance over which a material property has a relatively similar, but random values, and is used to model the spatial variation of the properties along the length of the deck.

The distribution, mean, and standard deviation for the diffusion coefficients of the substrate and the rigid overlay were taken from the experimental results described in Section 5.1, and correspond to a concrete with 5% of air content. The distribution and statistics for the diffusion coefficient of the patch were also obtained from the experimental study of Section 5.1. The statistics for the diffusion coefficient of the thin deck overlay were computed from the data provided in the Table 6.1 of the report by Vancura (2018). The spectrum and the correlation length of all diffusion coefficients were taken from Kerźner et al. (1998). The critical chloride threshold was characterized using the results of Table 1 in the study by Alonso and Sanchez (2009), obtained from natural tests for total chloride concentration. The statistics of the surface chloride concentration amplitude and deposition rate were obtained as described in Section 5.3 for two bridges in Indiana; their correlation lengths were taken from Karimi (2002) as reported in Table 2 of Botte et al. (2025). The statistics of the concrete cover were obtained from GPR data for a bridge in Indiana as explained in Section 5.2. We must note that in using GPR data for estimating rebar cover values, a permittivity value must be assumed for the tested concrete, as indicated in Equation 5.1. Since the scope of this study is to evaluate the impact of defective void content, we computed the statistics of the rebar cover using a low permittivity value of 5, which corresponds to very dry concrete, to obtain a mean value above INDOT's standard of 2.5 in. (63.5 mm). The correlation length of the concrete cover was estimated from the experimental power spectral density computed from the GPR data. Finally, the compressive strength was modeled with statistics and spectrum from Xu and Li (2018).

To model the distribution of voids along the length, we use Beta distributions. INDOT's tolerance value for air content is 6.5 ± 1.5% (INDOT, 2022b). For the standard case, we set a mean of 6% and standard deviation of 0.5%, which ensures that practically all of the values along the length of the deck fall within INDOT's tolerance. For the substandard case, the mean is 7.2% and the standard deviation is 0.5%. These settings for the substandard case yield between 5% and 8% of the void content values along the deck to be outside INDOT's tolerance. That is, between 5% and 8% of the area of the deck has an air content above INDOT's tolerance limit of 8%.

The air content values along the deck used in this case study are shown in Figure 6.2 for the standard and substandard cases. The x-axis represents the bridge length span in feet, and the y-axis shows the variation of the air content along the span. For the substandard case, the air content distribution is above INDOT's upper tolerance value, 8%, in 5.33% of its surface, which is close to the impact echo test results of the deck serving as a case study, where 5.2% of the tested surface was reported to have weak concrete. We assume that the regions of the deck violating INDOT's upper tolerance limit for air content are prone to develop visible honeycombs at the surface due to the high amount of entrapped air. For such points with

(a)

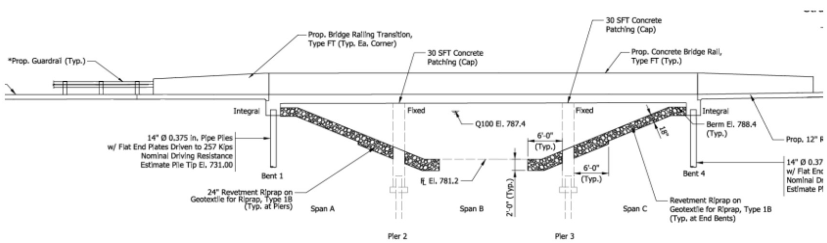

(b)

(c)

Figure 6.1 Asset 030-43-04852 CEBL: a) Photo When the One-Way Continuous Slab Bridge Superstructure Replacement Was Newly Opened to Traffic, b) Elevation Drawing, and c) Voids at the Bottom of the Slab.

TABLE 6.1
Summary of the Most Relevant Parameters of the Deterioration Model.

Parameter	Distribution	Spectrum	Mean	St. Dev.	Correlation Length
Diffusion coefficient (substrate and rigid overlay)	Weibull	Gaussian	0.50 in^2/year	0.08 in^2/year	1.64 ft
Diffusion coefficient (patch)	Weibull	Gaussian	0.75 in^2/year	0.23 in^2/year	1.64 ft
Diffusion coefficient (thin overlay)	Weibull	Gaussian	0.05 in^2/year	0.04 in^2/year	1.64 ft
Critical chloride threshold	Lognormal	Exponential	7.97 lb/ yd^3	5.60 lb/yd^3	6.56 ft
Surface chloride (amplitude)	Lognormal	Gaussian	16.56 lb/yd^3	1.31 lb/yd^3	6.42 ft
Surface chloride (deposition rate)	Lognormal	Gaussian	0.36 yr^{-1}	0.06 yr^{-1}	6.42 ft
Concrete cover	Lognormal	Exponential	2.89 in.	0.26 in.	3.61 ft
Compressive strength	Lognormal	Exponential	4.76 ksi	0.32 ksi	2.43 ft
Void content (standard)	Beta	Gaussian	6%	0.54%	1.64 ft
Void content (substandard)	Beta	Gaussian	7%	0.57%	1.64 ft

visible defects, we assume immediate intervention with patching shortly after construction.

The design and construction data of the one-way solid slab bridge are summarized in Table 6.2. These data were taken from the bridge drawings and confirmed in conversations with INDOT personnel. The milling, shot blasting, and patching depths vary along the deck's surface depending on the condition of the concrete at the time of the intervention. Here, for modeling purposes, we take typical, representative values of shot blasting and milling depth, and a conservative value of 1 in. below the rebar for the patching depth. It should be pointed out that these depths can be adjusted in the model to assess the effect of using other depth values, or of having varying depths. For this example, we use the values indicated in Table 6.2 as fixed, nonvarying parameters.

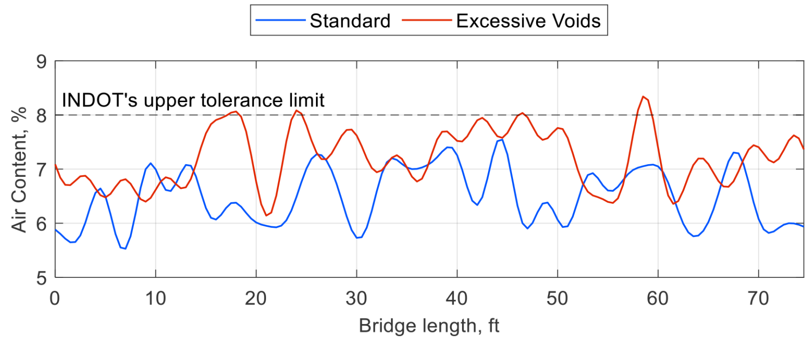

Figure 6.2 Variation of Air Content Values Along the Span of the Deck: Standard and Substandard Cases.

TABLE 6.2
Design and Construction Properties for the Illustrative Case Study.

Property	Value
Bridge length	75 ft
Section depth	16 in.
Rebar diameter	1 in.
Section width	0.5 ft
Curing time	28 days
Milling depth for rigid overlay	1 in.
Shot blasting depth for thin overlay	1/4 in.
Patching depth	3.5 in.

TABLE 6.3
Maintenance and Inspection-Related Parameters for the Illustrative Case Study.

Parameter	Value
Inspection period	2 years
Thin overlay application times	10 and 20 years
Rigid overlay application times	30 and 50 years
Minimum patching length	2 ft

The maintenance and inspection-related parameters considered in this illustrative case are shown in Table 6.3. Despite the model having the capability to trigger either state-based or scheduled interventions, as explained in Section 4.4, here only scheduled interventions are used. Accordingly, the application of thin and rigid deck overlays occur at the prescribed years shown in Table 6.3. Moreover, it is assumed that: (1) patching only occurs at the same time as the application of rigid and thin deck overlays; and (2) a fixed intervention schedule of two thin and two rigid overlays sequentially are applied at the times outlined in Table 6.3. Other intervention schedules and criteria can be used as inputs to study the impact on the estimated service life and costs. For example, one could specify two thin overlays and a single rigid, or a thin overlay at year 15 instead of year 10 if the deck is performing well. However, considering changes to prescribed practices is not within the scope of this report. Note that other intervention actions, such as crack sealing, are out of the scope of this project.

The condition rating assignment criteria outlined in Table 4.1, which comes from INDOT's (2022a) *Bridge Inspection Manual*, do not cover all possible cases. Specifically, the following cases are excluded from the assignment criteria:

- Cracking less than 0.012 in. and closely spaced
- Cracking less than 0.016 in. and closely spaced
- Cracking less than 0.020 in. and closely spaced
- Cracking greater than 0.020 in., less than 0.040 in., and widely spaced

For modeling purposes, we assigned the missing cases to the immediately lower case in Table 4.1. For example, the missing case 1 was assigned a condition rating of 8, and the missing case 4 was assigned a condition rating of 5.

6.2 Outputs of the Model

Using the inputs described in Section 6.1 with the model described in 4, a 70-year simulation of the bridge selected for this case study is performed. A single simulation generates more than 30 physical outputs that include, for each time of the simulation and for each point along the length of the deck, chloride profiles at each point of the length of the deck, variation of the diffusion coefficient values over time, times to initiation and cracking for each point in the deck, corrosion current density at the rebar, and rebar diameter loss due to corrosion. In this illustrative case, two key physical outputs are selected to plot, chloride profiles and crack width.

Figure 6.3 shows the penetration of the critical chloride threshold, that is, the penetration of the chloride concentration that will trigger rebar corrosion, for both the standard and substandard cases. First, we consider a point in time that is 9.5 years after the construction. At this time, the critical chloride threshold values are, taken as an average along the length of the deck, 9.4 lb/yd^3 for the standard case, and 4 lb/yd^3 for the substandard case. The lower tolerance of the substandard case to the action of chlorides is a consequence of the increased air content, as shown in Equation 4.9. In the substandard case, the critical chloride penetration has reached the top rebar in most locations, with a peak of concentration at around 18 ft that coincides with one of the air content peaks of Figure 6.2. Note that these peaks correspond to regions of the deck where

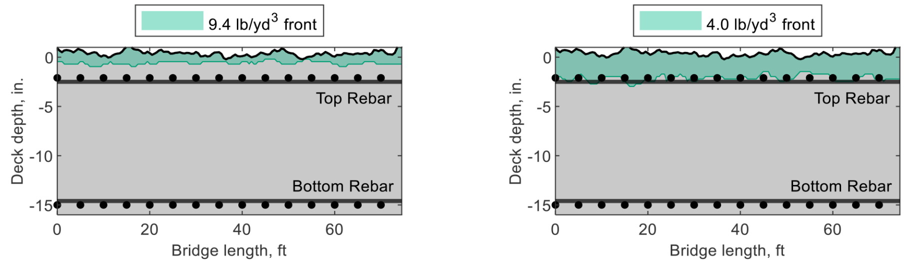

(a) Standard Case at 9.5 Years From Construction

(b) Substandard Case at 9.5 Years From Construction

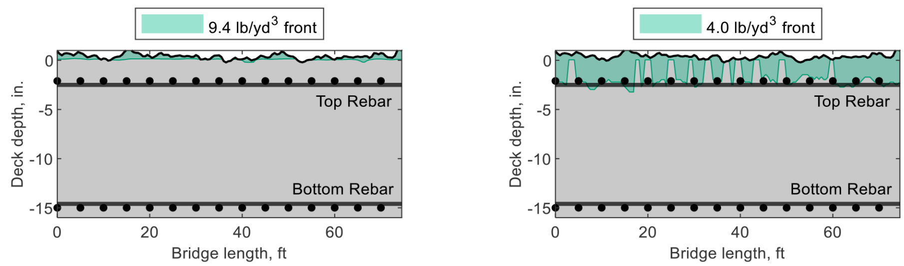

(c) Standard Case at 10.5 Years From Construction

(d) Substandard Case at 10.5 Years From Construction

Figure 6.3 Critical Chloride Penetration Front Before and After the Application of the First Thin Deck Overlay 10 Years After Construction.

honeycombing was identified and patched. In contrast, the critical penetration of the standard case is farther away from the rebar at this point in time.

The first thin deck overlay is scheduled for year 10 after construction. As described in Section 2.1.1, applying a thin deck overlay includes patching of areas with cracking, limited to 10% of the deck's area. As assumed for this illustrative case study, the depth of the patch is 1 in. below the rebar level. Thus, any existing chlorides from the surface to a depth of 3.5 in. are removed due to the concrete substitution. Similarly, any cracks in the patched regions are removed. The effect of the thin deck overlay can be seen in Figure 6.3c and 6.3d: superficial chlorides are removed via shotblasting in both the standard and substandard cases. For the substandard case, patching is applied in regions where corrosion cracking had weakened the concrete cover.

Figure 6.4a and 6.4b show the state of the deck at 19.5 years, shortly before the application of the second thin deck overlay. At this point in time the standard case exhibits significantly less cracking than the substandard case. The spikes indicate large cracking values caused by corrosion. Figure 6.4c and 6.4d then show the effect of the patching performed during the application of the second thin deck overlay. The large cracking values in Figure 6.4a and 6.4b are identified as regions of the deck with weakened concrete during shot blasting and, thus, are patched. Patching resets the cracking at the patched regions to zero, as seen in Figure 6.4c and 6.4d. Note that the need for patching in the standard case is minimal, while the substandard case needs more extensive work.

Figure 6.5 shows the condition rating number histories for both cases throughout 70 years. The percentage of patched area, patching cost, and cost of the overlays are also shown. The cost values were taken from INDOT's Pay Items List/Unit Price (INDOT, 2025). We can see that, in the substandard case, the condition rating drops to 7 two years earlier than the corresponding drop to 7 in the standard case. At the first thin deck overlay placement, the standard case does not require any patching, whereas the substandard case requires patching of 20% of the deck area. It must be pointed out that here the substandard case has more than 10% of its surface patched. According to INDOT's *Bridge Design Aids* (2020), thin decks are recommended on decks with patching expected in less than 10% of its surface. Thus, the substandard case illustrated here would require a different treatment. At the second deck overlay placement, the substandard case requires 46% of its area to be patched. Following Section 412-3.02(04) INDOT's *Bridge Design Manual* (2013), a deck needing more than 35% of its surface patched must be replaced. Here, because we are using the same intervention schedule in both cases for illustration, we assume that the deck is extensively patched and the second thin deck overlay is applied. Despite the early intensive patching applied at each intervention, which means that large portions of the weakened concrete were shot blasted, the substandard case has lower condition rating numbers overall than the standard case. Using the parameters and maintenance policies chosen in this illustrative case study, the total cost of maintenance for the substandard case is \$197,000, whereas for the standard case is \$157,000. Note that the amounts are intended to reflect a relative cost. Hence it could be said that the substandard case resulted in a 25% increase in maintenance costs, while holding everything else unchanged, and not accounting for a potential

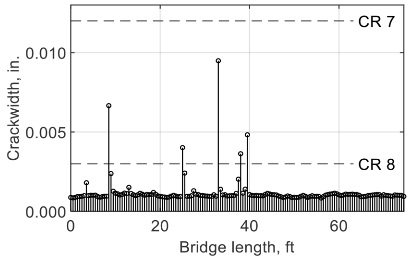

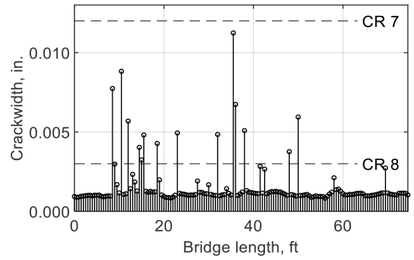

(a) Standard Case at 19.5 Years From Construction

(b) Substandard Case at 19.5 Years From Construction

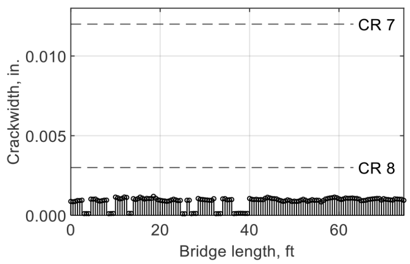

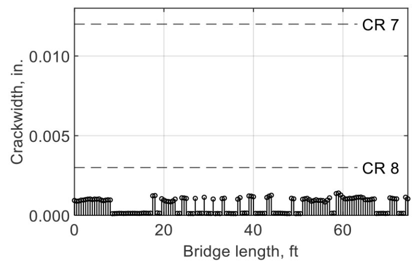

(c) Standard Case at 20.5 Years From Construction

(d) Substandard Case at 20.5 Years From Construction

Figure 6.4 Cracking Along the Deck Before and After the Application of the Second Thin Deck Overlay 20 Years After Construction.

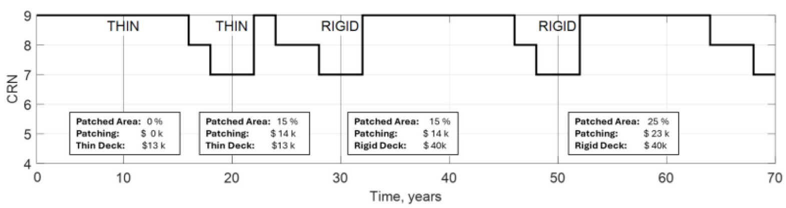

(a) Standard Case

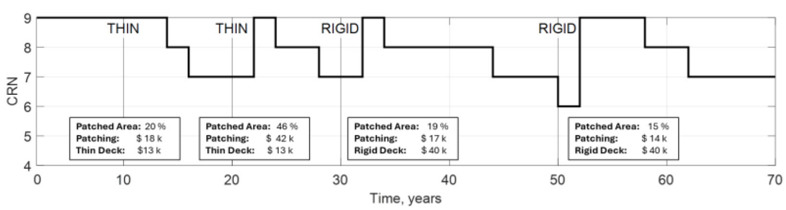

(b) Substandard Case

Figure 6.5 Condition Rating Number Histories Throughout the 75-Year Simulation Period.

early replacement of the substandard deck at year 20, which would represent a loss of life of 50 years.

The model captures the spatial variability of the deterioration process along the span of the bridge. When an intervention threshold is reached, the affected area is repaired. This process helps prevent substantial strength loss because the period during which rebar diameter can degrade is limited, once the surrounding concrete is patched, further degradation stops. Due to the inherent variability of the corrosion process, some locations experience more advanced deterioration than others. An unfortunate and inherent problem arises when deterioration occurs in regions of negative moment (tension at the top of the slab over interior supports): the resulting strength loss becomes critical for the bridge, as illustrated next.

Figure 6.6a illustrates the bending moment strength loss caused by deterioration at a specific location, assumed here to

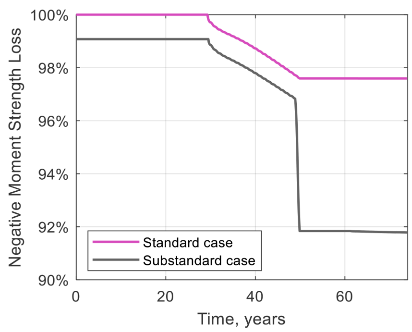

(a)

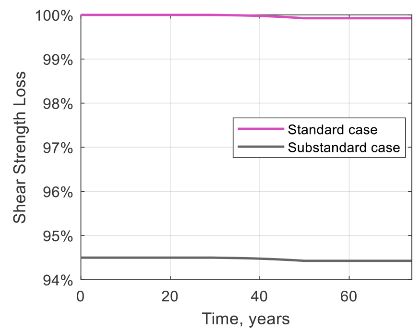

(b)

Figure 6.6 Strength Loss Comparison Due to Negative Bending Moment and Shear, at a Critical Location of the Bridge.

be a critical negative-moment region. In the substandard case, the presence of a larger number of voids leads to weaker concrete, therefore, a reduction in capacity is observed from year 0. Consequently, the bond strength given by Equation 2.4 is reduced compared to the standard case. This reduction causes the bond strength (see Equation 2.5) to become critical earlier in the bridge's service life than the degraded tensile capacity of the reinforcing bar. This behavior can be observed in Figure 6.6a, where a sudden drop appears at approximately 50 years. In contrast, the standard case does not exhibit such a drop because the bond strength remains greater than the degraded tensile capacity for a sufficient period, allowing the intervention to occur before bond failure becomes critical.

Similarly, Figure 6.6b shows the loss of shear strength. As shown in the figure, the difference in strength loss between the two cases is mainly a result of the presence of voids on the concrete compressive strength since year 0; deterioration of the reinforcement does not have as significant an impact as it does on the bending moment capacity. This point is evident in Equation 2.14 where the reinforcement ratio is less influential than the compressive strength in the calculation of shear strength when stirrups (shear reinforcement) is not provided.

This strength loss can be translated into an earlier reduction in the load rating of the substandard case over the bridge's service life compared to the standard case. It is important to note that load-rating analysis is complex and must be coupled with the outputs of this model to predict future load-rating degradation with any reasonable level of confidence.

7. CLOSING REMARKS

The objective of this research project was to provide INDOT with a methodology to enable the quantification of additional costs when construction defects are present in the bridges in the scope of this study. The form of those defects was specified to be an excessive number of air voids in the concrete bridge, and to also consider the impact of interventions that would be considered during the service life of the bridge on those life-cycle costs.

This research benefits the state of Indiana by:

- Providing INDOT with a quantitative approach to estimate the service life of the bridges, thus enabling INDOT to estimate several key metrics of condition such as estimates of chloride penetration, rate of bar corrosion, impact of the presence of voids and interventions and to estimate economic losses associated with the premature deterioration of concrete decks;
- Providing a physics model-based process for decision makers to make informed choices regarding maintenance strategies and investments, thus optimizing resource allocation and reducing economic losses over time;
- Potentially minimizing road closures through the reduction of construction activities derived from unplanned repairs and interventions, thus improving the traffic flow and overall mobility for road users; and
- Raising awareness of the impact of defective construction practices that trigger deterioration processes and shorten the lifespan of concrete decks or lead to unplanned interventions.

All of these points contribute to better network-level planning and budgeting. By accurately estimating the lifespan of concrete decks, INDOT can develop comprehensive maintenance and rehabilitation programs that align with the projected needs of the bridge inventory.

7.1 Final Recommendations

A summary of the major lessons learned and opportunities identified during this research is provided below. These are organized under the three major themes of: (i) Construction, Inspection, and Maintenance Practices; (ii) Data Acquisition and Testing; and (iii) Model Implementation

7.1.1 Construction, Inspection, and Maintenance Practices

A. The testing program described in Section 5.1 showed that patched concrete tends to have higher and less consistent diffusion coefficient values than sound concrete, which in contrast, shows lower typical values and has more predictable performance. This outcome translates into chlorides penetrating faster through patched concrete and hastening deterioration. Currently, the application of epoxy materials or primers in the cold joints between the patch and the surrounding concrete is not enforced. It is strongly recommended that INDOT call for the application of some bonding/sealing material when implementing a patch.

B. The case study described in 6 illustrated the consequences of improper concrete casting practices leading to concrete with higher air content. Only the honeycombs, which appear in 6.67% of the surface of the deck, are visible. As discussed in Section 4.5, key durability and strength-related properties are affected by excessive air content, even when it is not visible in the form of large voids. Excessive air content in the form of voids degrade the concrete bridge performance as shown in Figure 6.3, Figure 6.4, and Figure 6.5. Excessive air content affects the permeability of concrete, as well as its compressive strength and derived mechanical properties. This behavior results in faster corrosion-induced cracking. Therefore, it is recommended that concrete not complying with INDOT specification of 6.5 ± 1.5% when tested with the pressure method during pouring be rejected. Adhering to minimum slump practice is also very important in facilitating proper consolidation during concrete casting. Simulation outcomes also suggest that for bridges with voids or out-of-standard air content, thin epoxy overlays could be applied earlier than the usual 10-year period to prolong the life of the existing deck by slowing down chloride penetration.

C. One of the goals of applying a thin deck overlay is to prevent a loss in the condition rating number until the next overlay application. However, simulations show that, despite the thin deck overlay slowing down the penetration of chlorides, it would not stop ongoing corrosion in the rebar. Figure 6.5a shows that in the standard case, the first thin deck overlay does not prevent the condition rating from falling to 6. INDOT personnel noted that a thin deck overlay makes it difficult to visually identify any cracks underneath due to the shadowing that the stones project onto the surface. The perception that a thin deck overlay prevents the condition rating from falling could simply be related to the fact that it is more difficult to detect existing cracks in a deck after the thin overlay has been applied. It is suggested that INDOT take into account the presence of a thin deck overlay when conducting a visual inspection of the deck.

7.1.2 Data Acquisition and Testing

In a previous JTRP project, SPR-4526 (Criner et al., 2023), it was recommended that INDOT considered collecting data useful to improve the accuracy of the physics-based model developed. In the execution of the current project, the research team was provided with a data set containing chloride profiles, as recommended in SPR-4526. Similarly, the experiments performed in this project focused on obtaining the chloride diffusion coefficient of concrete with INDOT's specifications, which is a parameter we also recommended obtaining in SPR-4526. Moreover, we were provided with GPR datasets that enabled the characterization of the distributions of realistic concrete cover values. This additional data allowed us to perform simulations using data relevant to Indiana bridges. Interviews and discussions with INDOT personnel also provided valuable information to better capture typical inspection and maintenance processes across the state.

Despite these significant improvements, we would recommend additional data be collected that could improve the accuracy of the predictions. Next, we summarize our recommendations for data collection.

D. In this project, laboratory tests were performed to obtain the appropriate diffusion coefficient to use both for concrete with and without excessive voids, and concrete with and without patching. However, it is generally agreed that laboratory and in-situ diffusion coefficient and other chloride penetration related properties tend to vary (Alonso & Sanchez, 2009; Angst et al., 2022). In general, in-situ data collection campaigns for the following parameters and variables would be beneficial, especially if bridge-specific results are desired:
   - Chloride profiles
   - Corrosion current densities or half-cell potentials
   - Compressive strength
   - Average crack width

E. Predicting the state of a specific bridge in the future requires understanding the trends of the conditions affecting it over time. Given the long-term nature of the deterioration processes in bridges, some variables and parameters are not suitable for testing in a laboratory and should rely on a long-term monitoring program instead. For instance, all the parameters listed in Recommendation D are time-dependent quantities. Of those, measuring chloride profiles, corrosion current densities, and average crack width over time would significantly improve the accuracy of any simulations.

F. In this project, we extended the model developed in SPR-4526 from a "single-cell" model to a "strip-model". Rather than assuming that a small-size portion of the deck is representative of the entire deck, the model captures the variations in performance over the length of the deck. This change to a spatially varying model enabled incorporating the effects of inspection and maintenance practices into the results. However, as mentioned in Recommendation G in 7.1.3, this improvement requires understanding the trends of the model's inputs over the span of the deck. For this purpose, we recommend using several measurement points along the deck in the long-term data collection plan.

7.1.3 Model Implementation

The model developed in this project can now be employed to carry out simulations of long-term deterioration for a given bridge, estimating condition ratings, visible crack widths, loss of structural capacity, among other relevant variables, over the span of the bridge rather than at a single point. The model incorporates two types of variability: from one point to another within the same bridge, and from one bridge to another. In this report, the focus was on simulating a single realization for purposes of illustrating the approach in Section 6. However, the model has the capability to run several realizations to reflect how the variability of each input affects typical performance metrics: visible cracking, condition rating numbers, and costs. The model also captures the effect of a given intervention schedule on the bridge deterioration. It is possible to define the desired maintenance schedule based either on experience or on a desired performance criterion, and then use the outcomes of the model to support a recommended maintenance strategy.

In addition to the construction defects studied previously in SPR-4526, the model captures the effects of voids in the concrete. This expansion enables meaningful comparisons of deterioration patterns between a bridge with early-age defects and a standard, well-constructed bridge. The illustrative case study in 6 showed that voids cause the structure to exhibit signs of deterioration much earlier, requiring a greater investment in interventions than in the standard case. Moreover, by incorporating strength degradation, the model can estimate the loss of structural capacity in the section due to deterioration. Some recommendations on the proper use and potential further extensions of the model are summarized below.

G. The developed model is intended to serve as an estimation methodology for relative comparisons among different scenarios and to support asset management decisions. It is not intended as a replacement for a comprehensive physical assessment or a formal economic analysis, but rather to inform such decision.

H. The model provides structure-specific results when detailed parameters of the studied structure are used as inputs. The model currently runs in MATLAB, using a set of functions and scripts that process commands within the MATLAB environment and generate plots using MATLAB's built-in capabilities. It currently lacks a user interface, script optimization, and user-interface for non-experts. However, several cases are already programmed. The selection of and application of scheduled and state-based interventions is also automated, with the model automatically updating after each maintenance action. Automating the selection and execution of different bridge scenarios based on input from a non-expert user will require additional development time.

I. To prepare the model for full access and utilization, an implementation project would be desirable to compile the scripts and functions created in this project into a user-friendly application and provide a manual to define the inputs and explain how those data should be gathered. This application and the associated user manual would allow users to easily analyze various bridge decks, intervention schedules, and void configurations.

7.2 Implementation Plan

An implementation plan is proposed based on the outcomes of this research and supported by the final recommendations delineated in 7.1. The proposed aspects of the implementation plan include:

- Support a follow-up implementation effort focused on developing a user-friendly interface, an instruction manual, and training materials to facilitate the appropriate use of the model by INDOT personnel (Recommendations H and I).
- Enforce the application of bonding materials when implementing a patch (Recommendation A).
- Assess the long-term impact of placed concrete that does not comply with INDOT's air content specification of 6.5 ± 1.5% as per the pressure method results performed in the pouring site (Recommendation B), if not rejected.
- Test for hidden voids in decks whose concrete was accepted, but was near the upper tolerance limit, within one year of casting (Recommendation B).
- For decks with voids, schedule the first thin deck overlay application at least two years before the usual 10-year mark (Recommendation C).
- Evaluate procedures for inspection of decks with thin deck overlays, as well as the criteria for assigning condition rating numbers in the current version of the INDOT *Bridge Inspection Manual* (2020) (Recommendation D).
- Enhance the accuracy of the simulations generated with the model developed in this project by gathering additional data could be collected following Recommendations E to G.

REFERENCES

ACI Committee 318. (2005). *Building code requirements for structural concrete (ACI 318-05): Commentary on building code requirements for structural concrete (ACI 318R-05).* American Concrete Institute. https://www.concrete.org/Portals/0/Files/PDF/Previews/318-05_preview.pdf

ACI Committee 318. (2005). *Metric building code requirements for structural concrete (ACI 318M-05): Commentary on metric building code requirements for structural concrete (ACI 318RM-05).* American Concrete Institute. https://www.concrete.org/publications/internationalconcreteabstractsportal/m/details/id/14676

ACI Committee 318. (2019). *Building code requirements for structural concrete (ACI 318-19): Commentary on building code requirements for structural concrete (ACI 318R-19)*. American Concrete Institute. https://www.concrete.org/Portals/0/Files/PDF/Previews/318-19_preview.pdf

ACI Committee 365. (2017). *ACI PRC-365.1-17: Report on service life prediction*. American Concrete Institute.

Ahmad, S., & Azad, A. K. (2013). An exploratory study on correlating the permeability of concrete with its porosity and tortuosity. *Advances in Cement Research*, *25*(5), 288–294. https://doi.org/10.1680/adcr.12.00052

Alonso, M. C., & Sanchez, M. (2009). Analysis of the variability of chloride threshold values in the literature. *Materials and Corrosion*, *60*(8), 631–637. https://doi.org/10.1002/maco.200905296

Al-Salloum, Y. (2007). Flexural performance of RC beams repaired with commercial repair materials. *Journal of King Saud University-Engineering Sciences*, *19*(2), 153–172. https://doi.org/10.1016/S1018-3639(18)30945-0

American Association of State Highway and Transportation Officials. (2022). Standard method of test for predicting chloride penetration of hydraulic cement concrete by the rapid migration procedure (AASHTO T 357-22).

American Association of State Highway and Transportation Officials. (2023). *Standard method of test for rapid determination of the chloride permeability of concrete* (AASHTO T 277-23).

American Concrete Institute. (2013). *CT-13: Concrete terminology*.

Angst, U. M., Isgor, O. B., Hansson, C. M., Sagüés, A., & Geiker, M. R. (2022). Beyond the chloride threshold concept for predicting corrosion of steel in concrete. *Applied Physics Reviews*, *9*(1). https://doi.org/10.1063/5.0076320

ASTM International. (2022). *Standard test method for air content of freshly mixed concrete by the pressure method* (ASTM C231/C231M-22). https://doi.org/10.1520/C0231_C0231M-22

ASTM International. (2024a). *Standard test method for density (unit weight), yield, and air content (gravimetric) of concrete* (ASTM C138/C138M-24a). https://doi.org/10.1520/C0138_C0138M-24A

ASTM International. (2024b). *Standard test method for microscopical determination of parameters of the air-void system in hardened concrete* (ASTM C457/C457M-24). https://doi.org/10.1520/C0457_C0457M-24

Azam, R., & Soudki, K. (2012). Structural performance of shear-critical RC deep beams with corroded longitudinal steel reinforcement. *Cement and Concrete Composites*, *34*(8), 946–957. https://doi.org/10.1016/j.cemconcomp.2012.05.003

Bertolini, L., Elsener, B., Pedeferri, P., & Polder, R. B. (2003). *Corrosion of steel in concrete: Prevention, diagnosis, repair*. Wiley. https://doi.org/10.1002/3527603379

Beushausen, H.-D., & Alexander, M. G. (2007). Performance of concrete patch repair systems. In C. U. Grosse (Ed.), *Advances in construction materials 2007* (pp. 255–262). https://doi.org/10.1007/978-3-540-72448-3_25

Botte, W., Vereecken, E., & Caspeele, R. (2025). Random field modelling of spatial variability in concrete: A review. *Structure and Infrastructure Engineering*, *21*(6), 1047–1060. https://doi.org/10.1080/15732479.2023.2248102

Cairns, J., Plizzari, G. A., Du, Y., Law, D. W., & Franzoni, C. (2005). Mechanical properties of corrosion-damaged reinforcement. *ACI Materials Journal*, *102*(4), 256–264. https://doi.org/10.14359/14619

Claisse, P. A. (Ed.). (2021). *Transport properties of concrete: Modelling the durability of structures* (2nd ed.). Woodhead Publishing. https://doi.org/10.1016/C2019-0-01493-8

Criner, N. M., Salmeron, M., Zhang, X., Dyke, S. J., Ramirez, J. A., & Wogen, B. E. (2023). *Predictive analytics for quantifying the long-term costs of defects during bridge construction* (Joint Transportation Research Program Publication No. FHWA/IN/JTRP-2023/08). Purdue University. https://doi.org/10.5703/1288284317615

Cusson, D. (2009). Durability of repaired concrete structures. In N. Delatte (Ed.), *Failure, distress and repair of concrete structures* (pp. 296–321). Woodhead Publishing. https://doi.org/10.1533/9781845697037.2.296

Czarnecki, L., Geryło, R., & Kuczyński, K. (2020). Concrete repair durability. *Materials*, *13*(20), 4535. https://doi.org/10.3390/ma13204535

Do, J.-Y., & Kim, D.-K. (2012). AHP-based evaluation model for optimal selection process of patching materials for concrete repair: Focused on quantitative requirements. *International Journal of Concrete Structures and Materials*, *6*, 87–100. https://doi.org/10.1007/s40069-012-0009-9

Du, Y. G., Clark, L. A., & Chan, A. H. C. (2005). Residual capacity of corroded reinforcing bars. *Magazine of Concrete Research*, *57*(3), 135–147. https://doi.org/10.1680/macr.2005.57.3.135

El-Sayed, A. K. (2017). Shear capacity assessment of reinforced concrete beams with corroded stirrups. *Construction and Building Materials*, *134*, 176–184. https://doi.org/10.1016/j.conbuildmat.2016.12.118

El-Sayed, A. K., Hussain, R. R., & Shuraim, A. B. (2016). Effect of stirrup corrosion on the shear strength of reinforced concrete short beams. *Journal of Civil Engineering and Management*, *22*(4), 491–499. https://doi.org/10.3846/13923730.2014.897990

Emberson, N. K., & Mays, G. C. (1996). Significance of property mismatch in the patch repair of structural concrete. Part 3: Reinforced concrete members in flexure. *Magazine of Concrete Research*, *48*(174), 45–57. https://doi.org/10.1680/macr.1996.48.174.45

Frontera, A., & Cladera, A. (2022). Long-term shear strength of RC beams based on a mechanical model that considers reinforcing steel corrosion. *Structural Concrete*, *24*(1), 25–40. https://doi.org/10.1002/suco.202200428

Fu, C., Huang, J., Dong, Z., Song, C., & Zhang, Y. (2023). Shear behavior of reinforced concrete beams subjected to accelerated non-uniform corrosion. *Engineering Structures*, *286*. https://doi.org/10.1016/j.engstruct.2023.116081

Global Modeling and Assimilation Office. (n.d.). *MERRA-2 surface temperature (2 m)* [Data set]. NASA Goddard Earth Sciences Data and Information Services Center. https://disc.gsfc.nasa.gov/

Han, S.-J., Joo, H.-E., Choi, S.-H., Heo, I., Kim, K. S., & Seo, S.-Y. (2019). Experimental study on shear capacity of reinforced concrete beams with corroded longitudinal reinforcement. *Materials*, *12*(5), 837. https://doi.org/10.3390/ma12050837

Han, S.-J., Ju, H., & Lee, D. (2022). Practical approach for estimating flexural strengths of corroded RC members considering bond strength degradation. *Structures*, *39*, 808–820). https://doi.org/10.1016/j.istruc.2022.03.072

Han, S. J., Lee, D., Yi, S. T., & Kim, K. S. (2020). Experimental shear tests of reinforced concrete beams with corroded longitudinal reinforcement. *Structural Concrete*, *21*(5), 1763–1776. https://doi.org/10.1002/suco.201900248

Hickson, R. I., Barry, S. I., Mercer, G. N., & Sidhu, H. S. (2011). Finite difference schemes for multilayer diffusion. *Mathematical and Computer Modelling, 54*(1–2), 210–220. https://doi.org/10.1016/j.mcm.2011.02.003

Imperatore, S., Rinaldi, Z., & Drago, C. (2017). Degradation relationships for the mechanical properties of corroded steel rebars. *Construction and Building Materials*, *148*, 219–230. https://doi.org/10.1016/j.conbuildmat.2017.04.209

Indiana Department of Transportation. (2013). *Indiana design manual.* https://www.in.gov/dot/div/contracts/design/IDM.htm

Indiana Department of Transportation. (2020). *Bridge design aids* (BDA 412-03). https://www.in.gov/dot/div/contracts/standards/bridges/BDA/BDA%20412_03%20Polymeric%20Overlay%20Considerations.pdf

Indiana Department of Transportation. (2022a*). INDOT bridge inspection manual*. https://www.in.gov/dot/div/contracts/standards/bridge_inspection/inspector_manual/Bridge_Inspection_Manual%20Rev_05182022.pdf

Indiana Department of Transportation. (2022b). *Standard specifications*. https://www.in.gov/dot/div/contracts/standards/book/sep21/2022%20Standard%20Specifications.pdf

Indiana Department of Transportation. (2025). *INDOT: Pay items list/unit price summaries*. https://www.in.gov/indot/doing-business-with-indot/home/contracts/standards/indot-pay-items-listunit-price-summaries/

Juarez, C. A., Guevara, B., Fajardo, G., & Castro-Borges, P. (2011). Ultimate and nominal shear strength in reinforced concrete beams deteriorated by corrosion. *Engineering Structures*, *33*(12), 3189–3196. https://doi.org/10.1016/j.engstruct.2011.08.014

Karimi, A. R. (2002). Probabilistic assessment of deterioration and strength of concrete bridge beams and slabs [PhD Thesis]. Imperial College London (University of London).

Kassir, M. K., & Ghosn, M. (2002). Chloride-induced corrosion of reinforced concrete bridge decks. *Cement and Concrete Research*, *32*(1), 139–143. https://doi.org/10.1016/S0008-8846(01)00644-5

Kerźner, Z., Novák, D., Rusina, R., & Teplỳ, B. (1998). Stochastic finite element method as a tool for modelling of deterioration of concrete structures*.* *Zeszyty Naukowe*, *42,* 27–36.

Kiani, B., Liang, R. Y., & Gross, J. (2018). Material selection for repair of structural concrete using VIKOR method. *Case Studies in Construction Materials*, *8*, 489–497. https://doi.org/10.1016/j.cscm.2018.03.008

Kim, M. O., Bordelon, A., Lee, M. K., & Oh, B. H. (2016). Cracking and failure of patch repairs in RC members subjected to bar corrosion. *Construction and Building Materials*, *107*, 255–263. https://doi.org/10.1016/j.conbuildmat.2016.01.017

Kirkpatrick, T. J., Weyers, R. E., Anderson-Cook, C. M., & Sprinkel, M. M. (2002). Probabilistic model for the chloride-induced corrosion service life of bridge decks. *Cement and Concrete Research*, *32*(12), 1943–1960. https://doi.org/10.1016/S0008-8846(02)00905-5

Kristiawan, S. A., Saifullah, H. A., & Supriyadi, A. (2021). Influence of patching on the shear failure of reinforced concrete beam without stirrup. *Infrastructures*, *6*(7), 97. https://doi.org/10.3390/infrastructures6070097

Kristiawan, S. A., Supriyadi, A., & Muktamirin, M. K. (2016). Effect of patching thickness on the flexural performance of patched reinforced concrete beams. In D.-K. Kim, J. Jung, & J. Seo (Eds.), *Advances in civil, architectural, structural and constructional engineering* (pp. 225–229). CRC Press. https://doi.org/10.1201/b19961

Kruczek, B. (2015). Carman–Kozeny equation. In E. Drioli & L. Giorno (Eds.), *Encyclopedia of MEMBRANES* (pp. 1–3). https://doi.org/10.1007/978-3-642-40872-4_1995-1

Kwon, S. J., Na, U. J., Park, S. S., & Jung, S. H. (2009). Service life prediction of concrete wharves with early-aged crack: Probabilistic approach for chloride diffusion. *Structural Safety*, *31*(1), 75–83. https://doi.org/10.1016/j.strusafe.2008.03.004

Lachemi, M., Al-Bayati, N., Sahmaran, M., & Anil, O. (2014). The effect of corrosion on shear behavior of reinforced self-consolidating concrete beams. *Engineering Structures*, *79*, 1–12. https://doi.org/10.1016/j.engstruct.2014.07.044

Malumbela, G., Moyo, P., & Alexander, M. (2011). Load-bearing capacity of corroded, patched and FRP-repaired RC beams. *Magazine of Concrete Research*, *63*(11), 797–812. https://doi.org/10.1680/macr.2011.63.11.797

Manawadu, A., Qiao, P., & Wen, H. (2023). Characterization of substrate-to-overlay interface bond in concrete repairs: A review. *Construction and Building Materials*, *373*. https://doi.org/10.1016/j.conbuildmat.2023.130828

Mangat, P. S., & O'Flaherty, F. J. (2000). Influence of elastic modulus on stress redistribution and cracking in repair patches. *Cement and Concrete Research*, *30*(1), 125–136. https://doi.org/10.1016/S0008-8846(99)00217-3

Mehta, K. P., & Monteiro, P. J. M. (2006). Concrete: Microstructure, properties, and materials (3rd ed.). McGraw-Hill.

Mindess, S., Young, F., & Darwin, D. (2003). *Concrete* (2nd ed.). Prentice-Hall.

Morgan, D. R. (1996). Compatibility of concrete repair materials and systems. *Construction and Building Materials*, *10*(1), 57–67. https://doi.org/10.1016/0950-0618(95)00060-7

Nordtest. (1999). *Concrete, mortar and cement-based repair materials: Chloride migration coefficient from non-steady-state migration experiments* (NT Build 492). https://www.nordtest.info/wp/1999/11/21/concrete-mortar-and-cement-based-repair-materials-chloride-migration-coefficient-from-non-steady-state-migration-experiments-nt-build-492/

Nounu, G., & Chaudhary, Z.-U.-H. (1999). Reinforced concrete repairs in beams. *Construction and Building Materials*, *13*(4), 195–212. https://doi.org/10.1016/S0950-0618(99)00014-8

Papakonstantinou, K. G., & Shinozuka, M. (2013). Probabilistic model for steel corrosion in reinforced concrete structures of large dimensions considering crack effects. *Engineering Structures*, *57*, 306–326. https://doi.org/10.1016/j.engstruct.2013.06.038

Pattnaik, R. R., & Rangaraju, P. R. (2007). Analysis of compatibility between repair material and substrate concrete using simple beam with third point loading. *Journal of Materials in Civil Engineering*, *19*(12), 1060–1069. https://doi.org/10.1061/(ASCE)0899-1561(2007)19:12(1060)

Pellegrino, C., da Porto, F., & Modena, C. (2011). Experimental behaviour of reinforced concrete elements repaired with polymer-modified cementicious mortar. *Materials and Structures*, *44*, 517–527. https://doi.org/10.1617/s11527-010-9646-0

Poursaee, A. (2016). Preface. In A. Poursaee (Ed.), *Corrosion of steel in concrete structures* (pp. xvii–xviii). Woodhead Publishing. https://doi.org/10.1016/B978-1-78242-381-2.05001-X

Ryan, T. W., Lloyd, C. E., Pichura, M. S., Tarasovich, D. M., & Fitzgerald, S. (2023). *Bridge inspector's reference manual (BIRM) (2022 NBIS)* (Report No. FHWA-NHI-23-024). National Highway Institute. https://rosap.ntl.bts.gov/view/dot/71829

Sahamitmongkol, R., Suwathanangkul, S., Phoothong, P., & Kato, Y. (2008). Flexural behavior of corroded RC members with patch repair-experiments & simulation. *Journal of Advanced Concrete Technology*, *6*(2), 317–336. https://doi.org/10.3151/jact.6.317

Saifullah, H. A., Supriyadi, A., Rizki, A., & Kristiawan, S. A. (2023). Influence of patching length on the flexural behaviour of patched reinforced concrete beam. *Journal of Engineering Science & Technology Review*, *16*(2). https://doi.org/10.25103/jestr.162.15

Salmeron, M., Criner, N., Zhang, X., Dyke, S. J., Ramirez, J. A., Wogen, B. E., & Rearick, A. (2024). Mechanistic modeling of construction defects in concrete decks subject to corrosion-induced deterioration. *Journal of Bridge Engineering*, *29*(9). https://doi.org/10.1061/JBENF2.BEENG-6636

Samples, L. M., & Ramirez, J. A. (2000). Field investigations of concrete bridge decks in Indiana: Part I: New construction & initial field investigation of existing bridge decks. *Concrete International*, *22*(), 59–63.

Sancharoen, P., Kato, Y., & Uomoto, T. (2008). Probability-based maintenance planning for RC structures attacked by chloride. *Journal of Advanced Concrete Technology, 6*(3), 481–495. https://doi.org/10.3151/jact.6.481

Shafikhani, M., & Chidiac, S. E. (2019). Quantification of concrete chloride diffusion coefficient–A critical review. *Cement and Concrete Composites*, *99*, 225–250. https://doi.org/10.1016/j.cemconcomp.2019.03.011

Shetty, M. S., & Jain, A. K. (2019). *Concrete technology: Theory and practice* (8th ed.). S. Chand Publishing.

Shiotani, T., Bisschop, J., & Van Mier, J. G. M. (2003). Temporal and spatial development of drying shrinkage cracking in cement-based materials. *Engineering Fracture Mechanics*, *70*(12), 1509–1525. https://doi.org/10.1016/S0013-7944(02)00150-9

Stewart, M. G., & Al-Harthy, A. (2008). Pitting corrosion and structural reliability of corroding RC structures: Experimental data and probabilistic analysis. *Reliability Engineering & System Safety*, *93*(3), 373–382. https://doi.org/10.1016/j.ress.2006.12.013

Tan, N. N., & Kien, N. T. (2021). An experimental study on the shear capacity of corroded reinforced concrete beams without shear reinforcement. *Journal of Science and Technology in Civil Engineering*, *15*(1), 55–66. https://doi.org/10.31814/stce.nuce2021-15(1)-05

Teixeira, O. G., Geraldo, R. H., da Silva, F. G., Gonçalves, J. P., & Camarini, G. (2019). Mortar type influence on mechanical performance of repaired reinforced concrete beams. *Construction and Building Materials*, *217*, 372–383. https://doi.org/10.1016/j.conbuildmat.2019.05.035

U.S. Environmental Protection Agency. (n.d.). *Ground penetrating radar (GPR).* https://www.epa.gov/environmental-geophysics/ground-penetrating-radar-gpr

Vancura, M. E., MacDonald, K. A., & Pilarski, P. (2018). *A rational method of surface treatment selections for concrete decks* (Report No. 2018–24). Minnesota Department of Transportation. https://hdl.handle.net/20.500.14153/mndot.3153

Vembu, P. R. S., & Ammasi, A. K. (2023). A comprehensive review on the factors affecting bond strength in concrete. *Buildings*, *13*(3), 577. https://doi.org/10.3390/buildings13030577

Wong, H. S., Pappas, A. M., Zimmerman, R. W., & Buenfeld, N. R. (2011). Effect of entrained air voids on the microstructure and mass transport properties of concrete. *Cement and*

Concrete Research, *41*(10), 1067–1077. https://doi.org/10.1016/j.cemconres.2011.06.013

Xu, T., & Li, J. (2018). Assessing the spatial variability of the concrete by the rebound hammer test and compression test of drilled cores. *Construction and Building Materials*, *188*, 820–832. https://doi.org/10.1016/j.conbuildmat.2018.08.138

Xue, X., Seki, H., & Song, Y. (2014). Shear behavior of RC beams containing corroded stirrups. *Advances in Structural Engineering*. *17*(2), 165–177. https://doi.org/10.1260/1369-4332.17.2.165

Ye, Z., Zhang, W., & Gu, X. (2018). Deterioration of shear behavior of corroded reinforced concrete beams. *Engineering Structures*, *168*, 708–720. https://doi.org/10.1016/j.engstruct.2018.05.023

Zhang, P., Li, D., Qiao, Y., Zhang, S., Sun, C., & Zhao, T. (2018). Effect of air entrainment on the mechanical properties, chloride migration, and microstructure of ordinary concrete and fly ash concrete. *Journal of Materials in Civil Engineering*, *30*(10). https://doi.org/10.1061/(ASCE)MT.1943-5533.0002456

About the Joint Transportation Research Program (JTRP)

On March 11, 1937, the Indiana Legislature passed an act which authorized the Indiana State Highway Commission to cooperate with and assist Purdue University in developing the best methods of improving and maintaining the highways of the state and the respective counties thereof. That collaborative effort was called the Joint Highway Research Project (JHRP). In 1997 the collaborative venture was renamed as the Joint Transportation Research Program (JTRP) to reflect the state and national efforts to integrate the management and operation of various transportation modes.

The first studies of JHRP were concerned with Test Road No. 1—evaluation of the weathering characteristics of stabilized materials. After World War II, the JHRP program grew substantially and was regularly producing technical reports. Over 1,600 technical reports are now available, published as part of the JHRP and subsequently JTRP collaborative venture between Purdue University and what is now the Indiana Department of Transportation.

Free online access to all reports is provided through a unique collaboration between JTRP and Purdue Libraries. These are available at docs.lib.purdue.edu/jtrp/.

Further information about JTRP and its current research program is available at engineering.purdue.edu/JTRP.

About This Report

An open access version of this publication is available online. See the URL in the citation below.

Salmeron, M., Forero, O., Faiz, T., Shrivastava, K., Dyke, S. J., & Ramirez, J. A. (2026). *Physics-based modelling of concrete degradation phenomena: Impact of construction defects on long term cost and material properties* (Joint Transportation Research Program Publication No. FHWA/IN/JTRP-2026/14). West Lafayette, IN: Purdue University. https://doi.org/10.5703/1288284318622